journal

J. Am. Ceram. Soc., **81** [3] 629–45 (1998)

Yttrium Aluminum Garnet Fibers from Metalloorganic Precursors

Yin Liu,* Zhi-Fan Zhang, John Halloran,* and Richard M. Laine*

Departments of Materials Science and Engineering, Chemistry, and the Macromolecular Science and Engineering Center, University of Michigan, Ann Arbor, Michigan 48109-2136

Mixtures of yttrium acetate hydrate ($Y(O_2CCH_3)_3 \cdot 4H_2O$) and aluminum formate hydrate ($Al(O_2CH)_3 \cdot 3H_2O$ in H_2O) or yttrium isobutyrate ($Y[O_2CCH(CH_3)_2]_3$) and aluminum isobutyrate ($Al[O_2CCH(CH_3)_2]_3$) in tetrahydrofuran were used as precursors to process yttrium aluminum garnet (YAG, $Al_5Y_3O_{12}$) fibers. The pyrolytic decomposition patterns of $Al(O_2CH)_3 \cdot 3H_2O$, $Y(O_2CCH_3)_3 \cdot 4H_2O$, and a [$3Y(O_2CCH_3)_3 \cdot 4H_2O/5Al(O_2CH)_3 \cdot 3H_2O$] YAG stoichiometry mixture were assessed by heating samples to selected temperatures and characterizing the products by thermogravimetric analysis, differential thermal analysis, X-ray diffractometry, and Fourier transform infrared spectroscopy. The YAG acetate/formate precursor decomposes to an amorphous intermediate at temperatures >400°C and crystallizes (at ~800°C) to phase-pure YAG with a ceramic yield of 40% at 1000°C. YAG isobutyrate precursor fibers were extruded or hand drawn. YAG acetate/formate precursor fibers were formed using a commercial extruder. The pyrolysis behavior of both precursor fibers was studied to identify the best pyrolysis conditions for producing dense, defect-free ceramic fibers. Only thin (diameter of <30 μm) precursor fibers could be processed to dense, defect-free, thin YAG fibers (diameter of <20 μm). For the YAG isobutyrate precursor, crack-free crystalline YAG fibers (diameter of ~7 μm) were obtained at 1000°C. For YAG acetate/formate precursor fibers, dwell times of 2 h at temperatures of 400° and 900°C were necessary to process fully dense, defect-free ceramic fibers. Heating the resulting 900°C fibers (at a rate of 30°C/min) to 1570°–1650°C gave dense fibers with grain sizes of 0.7–3.2 μm and bend strengths of up to 1.7 ± 0.2 GPa (for fibers that had a diameter of ~10 μm and had undergone sintering at 1600°C).

I. Introduction

YTTRIUM aluminum garnet (YAG or $Al_5Y_3O_{12}$) exhibits high strength and low creep rates at high temperatures (>1000°C) and, thus, offers potential for high-temperature structural applications.[1–4] In particular, YAG fibers may be of use for reinforcing ceramic-matrix composites (CMCs).[5] In fiber-reinforced CMCs, thin fibers (<20 μm) are desired because of their high strength, flexibility, and weavability.[6,7] Unfortunately, traditional ceramic processing methods (e.g., powder and melt processing) are usually not amenable to processing thin fibers (<20 μm in diameter).[1,6–10] Thus, chemical-processing approaches to ceramic fibers are now widely used.[1,11–14] For example, commercial Nicalon™ (10–12 μm in diameter; Nippon Carbon, Tokyo, Japan) and Tyranno™ (8–10 μm in diameter; Ube Industries, Yamaguchi, Japan) Si-C-O composite fibers are produced from polycarbosilane precursors.[8,15] Similarly, various commercial oxide fibers (most based on alumina (Al_2O_3) are produced using chemical-processing approaches. For example, Saffil™ Al_2O_3 fibers (diameter of ~3 μm, 5% silica (SiO_2); ICI, Runcorn, U.K.) are produced from $AlCl_3$ or aluminum acetate/polysiloxane precursors,[16] and Sumika Alumina™ fibers (diameter of ~17 μm, 50% SiO_2; Sumitomo Chemicals, Tokyo, Japan) are produced from alkyl-substituted polyaluminoxane/silicate ester precursors.[17] Both fiber microstructures are reported to consist of Al_2O_3 nanocrystals in an amorphous aluminosilicate matrix. The presence of an amorphous phase reduces the fiber tensile modulus, melting temperature, and creep resistance.[16]

The Nextel™ (The 3M Co., St. Paul, MN) series of Al_2O_3-based fibers (312, 440, 610, and 720, diameters of 10–12 μm) are made using aluminum monoacetate or formoacetate/silica hydrosol precursors.[18–22] The 3M patents describe methods of producing Al_2O_3 precursor fibers from spinnable solutions that consist of high concentrations of aluminum monoacetate (or aluminum formoacetate), lactic acid (or DMF), silica hydrosol, and small amounts of boric acid (H_3BO_3) (~2 wt%) or a hydrous iron polymer solution (~0.6 wt% Fe) in H_2O.[19,20] The extruded precursor fibers, on pyrolysis to temperatures >1000°C, exhibit composite microstructures that contain mixtures of microcrystalline (nanocrystalline) Al_2O_3 with mullite, silica–boria (SiO_2–B_2O_3), or aluminosilicates. The composite fibers exhibit melting points that are lower than that of Al_2O_3 because of the presence of lower melting phases, such as SiO_2, B_2O_3, or mullite. For example, Nextel™ 440 (70 wt% Al_2O_3/28 wt% SiO_2/2 wt% B_2O_3) melts at a temperature of ~1700°C, which is lower than that of Al_2O_3 (2054°C). Nextel™ 610 fibers (~99 wt% Al_2O_3/0.3 wt% SiO_2, grain size of ~0.1 μm) have a microstructure that consists of α-Al_2O_3 (major phase) with nanocrystalline mullite.[22] The presence of lower-melting mullite at Al_2O_3 grain boundaries can reduce the high-temperature performance of the fiber.[22]

In addition to Al_2O_3 fibers, other oxide fibers, including mullite, zirconia (ZrO_2), and SiO_2, have also been prepared using chemical routes.[23] Although many polycrystalline oxide fibers have been developed, most of them have a common drawback—i.e., low creep resistance at high temperatures.[22] The general reason is extremely fine grain sizes (<0.2 μm), which, coupled with the presence of a glassy phase, exacerbates creep. Consequently, dense, phase-pure ceramic fibers with larger grain sizes (0.5–2 μm for fibers that are 10–20 μm in diameter) are still needed for high-temperature engineering applications.

The choice of 0.5–2.0 μm grain sizes is suggested as a means of balancing high-temperature creep resistance with superior mechanical properties at all temperatures. This range of sizes represents a proposed rule of thumb that must be tested, because there are no literature studies on the effects of grain size on creep and mechanical properties for oxide ceramic fibers. Furthermore, because of the high surface-to-volume ratios

B. Dunn—contributing editor

Manuscript No. 191263. Received January 22, 1997; approved June 6, 1997.
Supported by the U.S. Air Force Wright Laboratory, Wright-Patterson Air Force Base (Wright-Patterson AFB, OH) through Contract Nos. F33615-91-C-5650 and FQ8671-9700732. Partially supported by the U.S. Office of Naval Research.
*Member, American Ceramic Society.

in ceramic fibers, it is not clear that such relationships, developed for monolithic materials, can be applied (see below).

Because YAG offers better high-temperature creep properties than Al_2O_3,[1–4] YAG fibers are potential substitutes for high-temperature engineering applications, as long as the above-mentioned concerns can be resolved. YAG fibers have been produced from the melt by crystal-growth methods. For example, Saphikon $Y_3Al_5O_{12}/Al_2O_3$ eutectic fibers (125 μm in diameter; Saphikon, Milford, NH) are produced using edge-defined film-fed growth (EFG) methods.[10,24] Single crystalline YAG fibers (800 μm in diameter) have been made using a laser-heated pedestal-growth (LHPG) method.[25]

Phase-pure, polycrystalline YAG fibers have also been made from suspensions of AlOOH and yttria (Y_2O_3) colloidal sols.[10] Fibers with diameters of ~120 μm and average grain sizes of ~4 μm were shown to offer bend strengths of ~520 ± 180 MPa and a bend stress relaxation (BSR) parameter of 0.92 (1100°C/1 h).[10] The obtained BSR is a factor of 10 greater than that of all commercially available polycrystalline Al_2O_3 fibers.[10]

The above-mentioned large-diameter, inflexible fibers are inconvenient for use in fiber-reinforced CMCs. Furthermore, single-crystal fibers are expensive and difficult to produce in quantity. Chen *et al.*[26] were able to produce thinner YAG fibers (diameters of 15–30 μm, grain sizes of 1.5 μm, and a BSR parameter of 0.95 at 1100°C/1 h) via sol–gel processing; however, small amounts of a second phase were added as a sintering aid, to improve fiber integrity.[26] Thus, phase-pure, fully dense, flexible YAG fibers still remain a viable processing target.

For this purpose, we recently described the use of yttrium and aluminum isobutyrates to synthesize YAG powders.[1] YAG fibers were also accessible;[27] however, this process required an inert environment (nitrogen gas or argon), because of the high moisture sensitivity and organic solvents (tetrahydrofuran (THF) and toluene) in aluminum isobutyrate. To simplify the process, we considered precursors that were less sensitive to air or moisture and were H_2O soluble. Yttrium acetate hydrate ($Y(O_2CCH_3)_3{\cdot}4H_2O$) and aluminum formate hydrate ($Al(O_2CH)_3{\cdot}3H_2O$) are both stable in air, dissolve in H_2O, and offer potential as starting materials for the synthesis of YAG fibers. In this paper, we describe (i) the reactivity patterns of $Al(O_2CH)_3{\cdot}3H_2O$, $Y(O_2CCH_3)_3{\cdot}4H_2O$, and 5:3 (Al:Y) stoichiometric mixtures of these compounds (YAG precursor) during their pyrolytic transformation to phase-pure Al_2O_3, Y_2O_3, and YAG, respectively; (ii) studies on fiber processing; and (iii) initial studies on the mechanical properties of YAG fibers from the formate/acetate precursor.

II. Experimental Procedure

(1) General Procedure

Aluminum tri(sec-butoxide) was purchased from Chattem Chemicals (Chattanooga, TN) and was used as received. Isobutyric acid (99%) was purchased from Pfaltz and Bauer (Waterbury, CT). Yttrium acetate hydrate (99.9%) ($Y(O_2CCH_3)_3{\cdot}xH_2O$) was purchased from Johnson Matthey Co. (Ward Hill, MA), and ethylene glycol (99%) was purchased from J. T. Baker (Phillipsburg, NJ). Formic acid (95%–97%) was purchased from Aldrich Chemical Co. (Milwaukee, WI). All the experiments were conducted in air.

(2) Synthesis and Characterization of YAG Precursor

(A) Synthesis of Aluminum Formate Hydrate $Al(O_2CH)_3{\cdot}3H_2O$ (FW = 216.081): Aluminum tri(sec-butoxide), $Al(OsBu)_3$, is 11 wt% aluminum (by thermogravimetric analysis (TGA)). In air, 75.09 g (306 mmol) of $Al(OsBu)_3$ was added to a 1000 mL beaker; 200.0 mL of H_2O (deionized, 11.11 mol, 12 equiv) was added to this material. The mixture gelled immediately as $Al(OH)_3{\cdot}3H_2O$ formed. Then, 60.0 g (1.30 mol, 1.42 equiv) of formic acid was added, partially dissolving the white gel. Another 300 mL of H_2O was added, and the mixture was heated, with stirring, to boiling. After 1 h, the white gel dissolved to a cloudy liquid. Boiling was continued (with stirring) to reduce the volume to ~100 mL. The temperature was then reduced to 60°C, to slow the evaporation rate. The beaker was covered with a watch glass to prevent contamination during evaporation. When the mixture became a wet white powder, it was further dried (drierite, SiO_2 gel) in a desiccator for 2 d. The yield was 65.9 g (306 mmol of $Al(O_2CH)_3{\cdot}3H_2O$), which is a 100% yield, based on the $Al(OsBu)_3$ that was consumed. The product was soluble in boiling water and gave a TGA (1000°C) ceramic yield of 23.6 wt% (theoretical yield is 23.6 wt%).

(B) Purification of Yttrium Acetate Hydrate, $Y(O_2CCH_3)_3{\cdot}4H_2O$ (FW = 338.10): Energy-dispersive spectroscopy (EDS) analysis showed trace amounts of chlorine and calcium in the purchased yttrium acetate. Therefore, 65 g of material was recrystallized from 500 mL of hot H_2O (100°C) and then filtered through coarse filter paper (P8, Fisher-brand, Fisher Scientific Hampton, NH). Evaporation at 100°C to ~150 mL gave a supersaturated solution (precipitates appeared) from which 56.4 g of crystalline product (87% yield, dried at 20°C/2 d/air) was recovered on cooling. No chlorine and calcium impurities were detected. The TGA ceramic yield was 33.5 wt% (theoretical yield is 33.4%).

(C) Preparation of YAG Precursor Solution: A 3:5 stoichiometric precursor solution, $3Y(O_2CCH_3)_3{:}5Al(O_2CH)_3$, was prepared by dissolving 11.63 g (34.4 mmol) of $Y(O_2CCH_3)_3{\cdot}4H_2O$ and 12.40 g (57.4 mmol) $Al(O_2CH)_3{\cdot}3H_2O$ in 350 mL of H_2O at 100°C in a 400 mL beaker. Formic acid (~6 g), ethylene glycol (4 g), and isobutyric acid (2 g) were added to stabilize the solution. The resulting solution was evaporated to reduce the volume to ~80 mL and then transferred to a rotary evaporator (Model RE-111, Brinkmann Instruments, Westbury, NY) to further reduce the volume until the viscosity was suitable for hand-drawing fibers (final volume of ~30 mL, TGA ceramic yield of 28%). Approximately 15 mL of YAG precursor solution was transferred to a 50 mL schlenk flask, then connected to a vacuum line and vacuum dried at 100°C (~0.75 torr (~100 Pa)) for 2 h. The dried precursor gave a TGA ceramic yield of 40.5% at 1000°C. After grinding in an Al_2O_3 mortar and pestle in air, the precursor was ready for bulk material studies.

(D) Density Measurements: Density measurements were used to establish the theoretical volume changes that are expected during the conversion from precursor to ceramic. Vacuum-dried, ground YAG precursor powders (~0.50 g) were pressed into disks that were 12.8 mm in diameter, using an applied pressure of 255 MPa for 15 s. The carboxylate complexes are assumed to deform plastically. Thus, the resulting pellet is assumed to be almost 100% dense. Optical microscopy suggests a fully dense material without visible porosity.[7] The dimensions of compacted pellets were measured (using calipers) to determine the densities. The average pellet dimensions were 12.86 mm × 2.42 mm, with a density of 1.5 g/cm^3.

(3) Pyrolysis and Characterization of the Bulk Precursor

(A) Pyrolysis Studies: Ground samples (~1 g) of $Al(O_2CH)_3{\cdot}3H_2O$, $Y(O_2CCH_3)_3{\cdot}4H_2O$, and the YAG precursor were placed in separate Al_2O_3 boats and heated in dry air at a rate of 10°C/min to selected temperatures, followed by a holding period of 2 h. Pyrolyses at temperatures <1000°C were conducted in a furnace (Type 6000, Thermolyne, Dubuque, IA) in flowing air (100 cm^3/min) that was equipped with a programmable temperature controller (Model 818P, Eurotherm, Northing, U.K.). Pyrolyses at 1400°C were conducted in another furnace (Model 51314, Lindberg, Watertown, WI) equipped with a controller (Model 59246-P, Lindberg).

(B) Thermogravimetric Analysis (TGA): TGA studies were performed using a thermal analysis instrument (Model Hi-Res TGA 2950, TA Instruments, New Castle, DE). The samples were loaded on a platinum sample pan. The TGA was

ramped at a rate of 10°C/min to 1000°C at the ''High-Res 4'' setting, with a nitrogen-gas balance flow of 40 cm^3/min and an air-purge flow of 60 cm^3/min.

(C) Differential Thermal Analysis (DTA): DTA experiments were conducted using a differential scanning calorimeter (Model DSC 2910, TA Instruments). DTA samples (10–20 mg) were loaded into a platinum crucible and heated at the same rate as the corresponding TGA Hi-Res sample rate, to 1500°C in dry air at a flow rate of 50 cm^3/min. The DTA reference was α-Al_2O_3 (Aluminum Co. of America, Pittsburgh, PA).

(D) Diffuse Reflectance Infrared Fourier Transform Spectroscopy (DRIFTS): DRIFTS studies were performed using a Fourier transform infrared spectroscopy (FTIR) spectrometer (Mattson Galaxy Series FTIR-3000, Mattson Instruments, Madison, WI). Optical-grade potassium bromide (KBr) crystal from International Crystal Laboratories (Garfield, NJ) was ground and used as the background. The experimental details have been described.[1]

(E) X-ray Diffractometry (XRD) Studies of Precursor Pyrolysis Products: The pyrolytic transformation of the precursors to crystalline products, as a function of processing temperature, was followed by X-ray diffractometry (XRD) using a rotating anode goniometer (Rigaku Denki Co., Tokyo, Japan). Samples (40–80 mg) were prepared using the same procedures as for the DRIFTS samples. The powders were then loaded into X-ray sample holders (glass plates) for data collection. The working voltage and current were 40 kV and 100 mA, respectively. Cu$K\alpha$ (λ = 1.54 Å) radiation with a nickel filter was used. Scans were continuous from 5°–80° 2θ, with a step scan of 10° 2θ/min and increments of 0.05° 2θ. Products (peak positions and relative intensities) were characterized by comparison with standard JCPDS† files.

(4) Fiber Studies

(A) Fiber Drawing and Extrusion: Precursor fibers were both hand drawn and extruded. For hand-drawn fibers, a small spatula was dipped into the viscous solution and withdrawn. The resulting fibers were suspended from a wooden framework (100 mm × 100 mm) and left to air dry. In this case, green fibers $\leq$20 μm in diameter and 200 mm in length were obtained.

Fibers were also extruded in air using an extruder (Bradford University Research, Bradford, U.K.). The extrusion spinneret diameter was 80 μm. Typically, 10 mL of precursor solution (ceramic yield of 27.9 wt%) was loaded into the chamber of the extruder. An extrusion load of 300–400 kg was applied to the piston to extrude fibers, with the extrusion-ram speed set at 0.05–0.15 mm/min. A rotating fiber takeup reel that was 250 mm in diameter and located 1 m below the spinneret allowed fiber drawing. Thinner or thicker fibers could be collected as a function of the takeup reel rotation speed, which could be varied from 0–10 rpm. The thinnest continuous fibers obtained were ~20 μm dia.

(B) Pyrolysis Studies of Fibers: All the $Al(O_2CH)_3{\cdot}H_2O$ and $Y(O_2CCH_3)_3{\cdot}4H_2O$ precursor fibers were dried at 100°C for 2 h, to remove the solvent, and then heated at a rate of 1°C/min to 400°C and held at that temperature for 2 h. The same Lindberg furnace that was used for bulk material studies was used for the high-temperature pyrolyses. All pyrolyses were conducted in air. Several heat-treatment schedules were studied: (i) heat treatment to remove carbonate by pyrolyzing fibers at 900° or 1000°C and holding them at that temperature for 2 h; (ii) different heating rates, such as 15°C/min and 30°C/min, for sintering; and (iii) sintering temperatures of 1400°, 1500°, 1550°, 1570°, 1600°, and 1650°C. Also, a batch of fibers were heat treated at a rate of 20°C/min to 1500°C for 2 h without dwelling at a temperature of 400°C for 2 h.

†Joint Committee on Powder Diffraction Standards, Swarthmore, PA (now International Center for Diffraction Data (ICDD), Newtowne Square, PA).

(C) Scanning Electron Microscopy (SEM): Green and pyrolyzed precursor fibers were characterized using a scanning electron microscopy (SEM) microscope (Model S800, Hitachi, Tokyo, Japan) that was operating at 5 keV. SEM samples were prepared by mounting fibers (3–5 mm in length) on an aluminum stub using carbon paste. The fibers were sputter coated with ~0.1 μm Au/Pd to improve the conductivity.

(D) Fiber Bend Tests: The strength of pyrolyzed fibers was evaluated using a ''bending test,'' as described in detail elsewhere;[28,29] this was done by forcing a YAG fiber sample to conform to a certain radius of curvature by looping it around drill bits or steel wires of decreasing diameters until the fiber failed. The diameters of the drill bits and wires that were used ranged from 2.5 mm to 0.5 mm. The fracture cross section of the broken fiber was then assessed by SEM, and the shortest distance from the centroidal axis to the surface of the fiber was recorded. The bend strength (σ) was then calculated using the relation

$$\sigma = \frac{Ez}{\rho}$$

where E is the elastic modulus (the value that was used is 280 GPa),[28] z the shortest distance from the centroidal axis to the surface of the fiber, and ρ the radius of curvature at which the fiber breaks.

III. Results and Discussion

In the following sections, we discuss (i) the synthesis and characterization of $Al(O_2CH)_3{\cdot}3H_2O$, $Y(O_2CCH_3)_3{\cdot}4H_2O$, and a formate/acetate YAG precursor, (ii) bulk pyrolysis decomposition patterns for the individual carboxylates and the YAG precursor, and (iii) preliminary studies on processing fibers from isobutyrate and formate/acetate precursors.

(1) Synthesis of $Al(O_2CH)_3{\cdot}3H_2O$

Aluminum formate hydrate was synthesized via the following reactions:[30,31]

$$Al(OCH_3CHCH_2CH_3)_3 + 3H_2O \xrightarrow{\text{room temp.}} Al(OH)_3 + 3HOCH_3CHCH_2CH_3 \quad (1)$$

$$Al(OH)_3 + 3HOOCH \xrightarrow{100°C} Al(O_2CH)_3 + 3H_2O \quad (2)$$

Reaction (2) provides different hydrate products, depending on the temperature at which water is removed, as discussed by Kwon[30] and Chaplygina *et al.*[31] When the final evaporation temperature is 105°C, the product is $Al(OH)(O_2CH)_2{\cdot}H_2O$, which is insoluble in H_2O, even at 100°C.[30] $Al(O_2CH)_3{\cdot}3H_2O$, which is obtained at ~65°C, dissolves slightly in H_2O.[31] $Al(O_2CH)_3{\cdot}4H_2O$, which is obtained at room temperature, dissolves in H_2O easily.[30] Anhydrous aluminum formate, $Al(O_2CH)_3$, is slightly soluble in cold H_2O but cannot be obtained via reaction (2).[30]

The $Al(O_2CH)_3{\cdot}3H_2O$ that has been produced here was formed at a temperature of ~60°C. The product is proposed to be $Al(O_2CH)_3{\cdot}3H_2O$, based on DRIFTS spectra and a found ceramic yield of 23.6%, which is the expected theoretical yield.

(2) Characterization of $Al(O_2CH)_3{\cdot}3H_2O$

(A) Thermal Analysis: The TGA profile for aluminum formate hydrate decomposition (Fig. 1) shows two regions of mass loss, from 20°C to 130°C and from 195°C to 300°C, with a final ceramic yield of 23.6 wt%. The first mass loss results in the loss of water and formic acid (reaction (3)):[22]

$$Al(O_2CH)_3{\cdot}3H_2O \xrightarrow{130°C} Al(OH)(O_2CH)_2{\cdot}0.5H_2O + HCOOH\uparrow + 0.5H_2O\uparrow \quad (3)$$

The ceramic yield at temperatures >130°C is 35.2 wt% Al_2O_3, which is similar to the theoretical yield for $Al(OH)(O_2CH)_2{\cdot}$

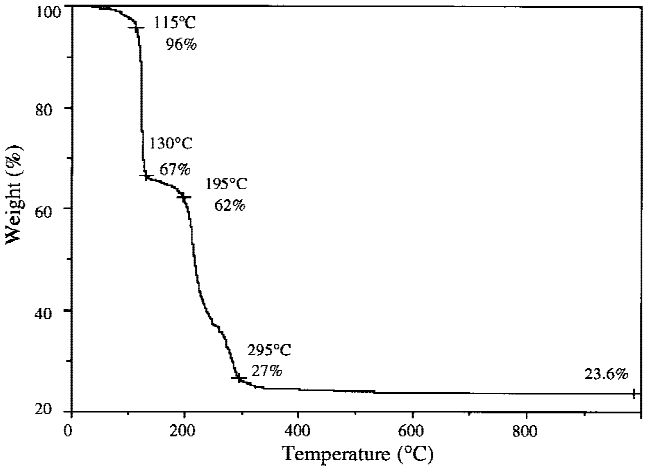

Fig. 1. TGA of $Al(O_2CH)_3{\cdot}3H_2O$ in air.

$0.5H_2O$ (35.6 wt%). $Al(OH)O_2CH)_2{\cdot}0.5H_2O$ formation is suggested by the DRIFTS studies below. At higher temperatures, $Al(OH)(O_2CH)_2{\cdot}0.5H_2O$ transforms to Al_2O_3:[30]

$$12Al(OH)(O_2CH)_2{\cdot}0.5H_2O \xrightarrow{340°C} 6Al_2O_3 + 5HCOOH\uparrow + 19CO\uparrow + 8.5H_2O\uparrow \quad (4)$$

Several intermediate decomposition products are proposed to form:[32]

$$Al(OH)(O_2CH)_2 \xrightarrow{200°C} Al_2O(O_2CH)_4 \xrightarrow{270°C} AlO(O_2CH) \xrightarrow{340°C} Al_2O_3 \quad (5)$$

The differential thermal analysis (DTA) that is shown in Fig. 2 reveals endotherms with maxima at 155° and 340°C. The endotherm that is centered at 155°C likely corresponds to reaction (3),[30] and the endotherm that is centered at 340°C likely corresponds to the decomposition of $Al_2O(O_2CH)_4$ and $AlO(O_2CH)$ (reaction (5)).[31,32]

DTA of the precursor does not provide clear details about high-temperature phase transformations because the sample size at temperatures >400°C is too small to compare with the reference Al_2O_3 (at 400°C, ~4 mg (20 wt%) remains). For this reason, a precursor sample was first pyrolyzed to 600°C for 2 h. Then, the same quantities of sample and reference (~20 mg each) were used to perform the DTA (5°C/min/air) to 1400°C to obtain the inset that is shown in Fig. 2. The inset shows two phase transformations: one that starts at 840°C and another that begins at 1120°C. The XRD data (Fig. 4) suggest that the 840°C exotherm corresponds to the crystallization of η-Al_2O_3, whereas the 1120°C exotherm corresponds to the crystallization of α-Al_2O_3. All the intermediate phases are white powders.

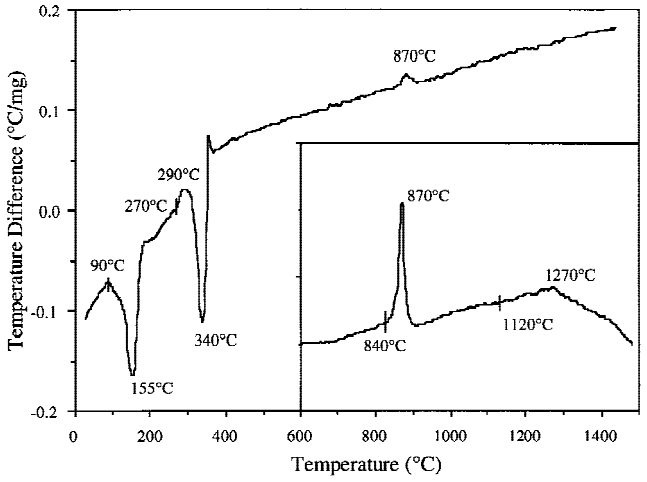

Fig. 2. DTA of $Al(O_2CH)_3{\cdot}3H_2O$ in air; the sample was heated at the same heating rate as TGA for $Al(O_2CH)_3{\cdot}3H_2O$ to 1000°C, then at 10°C/min to 1500°C.

(B) DRIFTS: The aluminum formate hydrate spectra that are shown in Fig. 3 (also see Table I) were analyzed and compared with published data.[23] The broad band at 3600–2300 cm^{-1} is assigned to ν(O−H) bands in the hydrate water.[23] The peak at 3500 cm^{-1} (ν(O−H)) in as-synthesized samples (very weak) and samples that have been pyrolyzed at 125°C indicates the presence of hydroxyl groups (Al−OH).[31] At 125°C, the spectrum is essentially identical to that reported for $AlOH(O_2CH)_3{\cdot}0.5H_2O$.[31]

In the 400°C spectrum, two slight peaks, at 1615 and 1390 cm^{-1}, indicate the formation of trace amounts of carbonate (CO_3^{2-}), e.g., $Al_2(CO_3)_3$.[1,33] The broad absorption bands indicate that the material is amorphous. The absence of a powder diffraction pattern via XRD suggests that the carbonate is either amorphous or of insufficient quantity to be detected (<2 wt%); this is corroborated by the TGA (Fig. 1), which shows a mass loss of ~1 wt% from 400° to 1000°C.

By 900°C, the carbonate bands disappear, coincident with the appearance of new absorption bands at 575 and 735 cm^{-1} that correspond to the appearance of η-Al_2O_3 in the XRD analysis.[1] In the DRIFTS spectra for samples that have been pyrolyzed at temperatures >1100°C, these peaks disappear and new peaks, at 470, 490, 620, and 650 cm^{-1}, appear that correspond to the appearance of α-Al_2O_3 in the XRD analysis.

(C) XRD Patterns: Figure 4 provides XRD data for $Al(O_2CH)_3{\cdot}3H_2O$ that has been heated (5°C/min/air) to selected temperatures for 2 h. The XRD pattern of the as-processed sample is crystalline. Although the pattern does not correspond to the diffraction data for $Al(O_2CH)_3{\cdot}3H_2O$,‡ it is quite similar to the XRD data from Chaplygina *et al.*[31]

At 125°C, the material remains crystalline; however, the powder pattern matches the diffraction data for $AlOH(O_2CH)_2{\cdot}xH_2O$.§ The ceramic yield from 125°C (35.2 wt% vs theoretical, 35.6 wt%) supports the formation of $AlOH(O_2CH)_2{\cdot}0.5H_2O$ as an intermediate.

The material becomes amorphous when heated to 400°C. At 900°C, the powder pattern reveals low-intensity, broad peaks that are indicative of the partial crystallization of η-Al_2O_3.¶ At 1100°C, as supported by the DTA data (Fig. 2), α-Al_2O_3‡‡ begins to crystallize. At 1400°C, a well-defined α-Al_2O_3 XRD pattern results, as indicated by the increasing intensity and the narrowing peak widths.

(3) Characterization of $Y(O_2CCH_3)_3{\cdot}4H_2O$

(A) Thermal Analysis: The $Y(O_2CCH_3)_3{\cdot}4H_2O$ that has been used in these studies was recrystallized to remove the calcium and chlorine impurities. Hussein[34] suggested the following thermal decomposition pattern:

$$Y(O_2CCH_3)_3{\cdot}4H_2O \xrightarrow{\sim 500°C} Y_2O_3 + Y_2(CO_3)_3 + \text{gases } (CO_2, CO, H_2O, CH_3COCH_3, \text{other})\uparrow \quad (6)$$

$$Y_2(CO_3)_3 \xrightarrow{>600°C} Y_2O_3 + CO_2\uparrow \quad (7)$$

The TGA profile (Fig. 5) shows two major mass losses. The first, from ambient to 85°C (~20 wt%), corresponds to the loss of H_2O. The second mass loss, from 265° to 340°C (~35 wt%), corresponds to the decomposition of the complex. At tempera-

‡JCPDS Powder Diffraction File Card No. 38-655.
§JCPDS Powder Diffraction File Card No. 37-771.
¶JCPDS Powder Diffraction File Card No. 16-394.
‡‡JCPDS Powder Diffraction File Card No. 10-173.

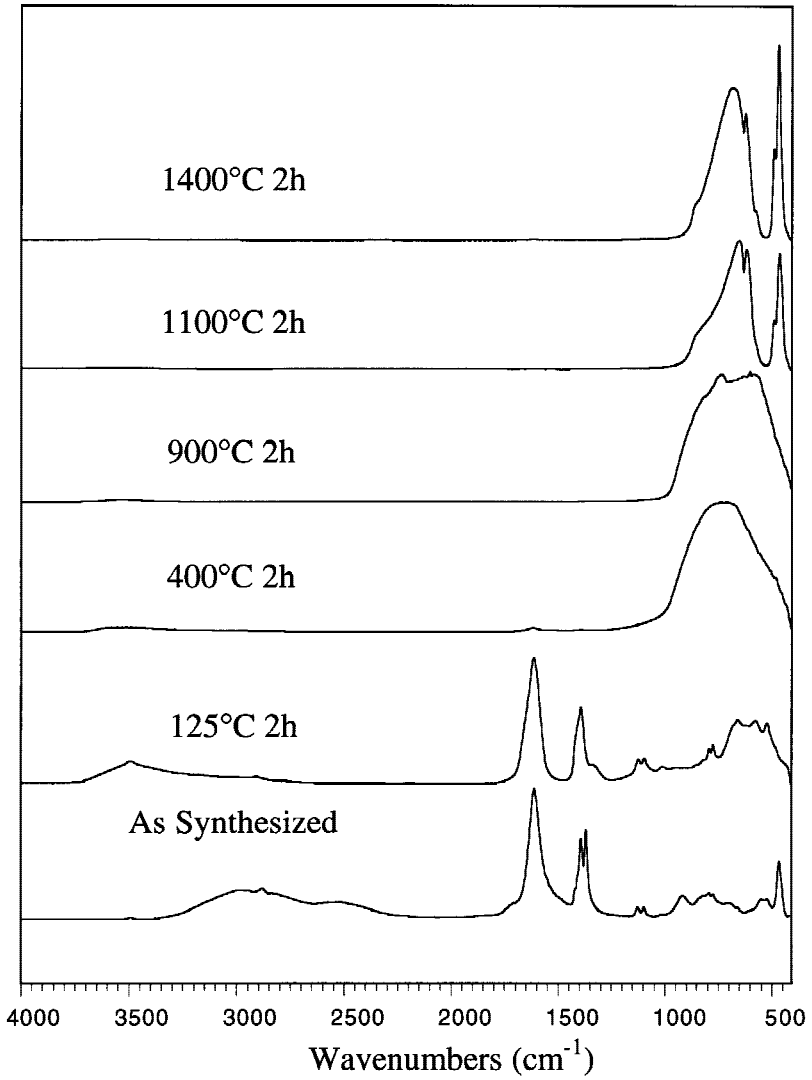

Fig. 3. DRIFTS spectra of $Al(O_2CH)_3 \cdot 3H_2O$ pyrolyzed at selected temperatures. Samples were ramped at 10°C/min in air to the selected temperature, with a holding time of 2 h.

Table I. IR Peaks of $Al(O_2CH)_3 \cdot 3H_2O$, $Y(O_2CCH_3)_3 \cdot 4H_2O$, and YAG Formate/Acetate Precursor

Compound	Wavenumber (cm^{-1})						
	ν(O−H)	ν(C−H)	ν_{as}(OCO)	$\nu_{as,def}$(OCO)	ν_s(OCO)	$\nu_{s,def}$(OCO)	ν_{def}(C−H)
$Al(O_2CH)_3 \cdot 3H_2O$†	3600–2300	2907	1620	1400	1375	800	
$AlOH(O_2CH)_2 \cdot nH_2O$†	3500	2930	1620	1420, 1406	1385	800	
$AlOH(O_2CH)_2$†	3500	2930	1630, 1605	1428, 1417	1400, 1390	800, 775	1080
$Al(O_2CH)_3 \cdot 3H_2O$	3600–2300	2900	1620	1400	1380	800, 780	
$Al(O_2CH)_3 \cdot 3H_2O$ at 125°C	3500	2910	1612	1391	1360	793, 774	
$Y(O_2CCH_3)_3 \cdot 4H_2O$	3600–2300	3010, 2960, 2950	1500	1450	1340		
YAG precursor	3600–2300	2880, 2950	1600, 1720 (tiny)	1464	1380		

†Data from Chaplygina *et al.*[31]

tures >340°C, TGA indicates a slow mass loss (~11 wt%) that corresponds to the evolution of CO_2 and some organics (see DRIFTS studies, section III(*3*)(*B*)). The ceramic yield (1000°C) is 33.5 wt% (Fig. 5), which exactly as calculated for $Y(O_2CCH_3)_3 \cdot 4H_2O$, given reactions (6) and (7). The ceramic yield of a sample that has been dried at 80°C for 2 h is 43.0 wt%, as calculated for conversion of $Y(O_2CCH_3)_3$ to Y_2O_3.

The DTA plot (Fig. 6) exhibits endotherms, starting at 50°C (centered at 100°C) and 250°C (centered at 300°C), and an exotherm at 340°C (maximum at 410°C). The 100°C endotherm likely corresponds to the loss of H_2O. The endotherm that is centered at ~300°C and the exotherm that is centered at 410°C correlate with the major mass loss. Based on the infrared (IR) results below and studies on $Al(O_2CCH_3)_3$ decomposition,[35] it is likely that the decomposition process involves ligand loss with some coincidental ligand oxidation, probably per the reactions

$$Y(O_2CCH_3)_3 \xrightarrow{\sim 300°C} YO(O_2CCH_3) + (CH_3CO)_2O \qquad (8)$$

and

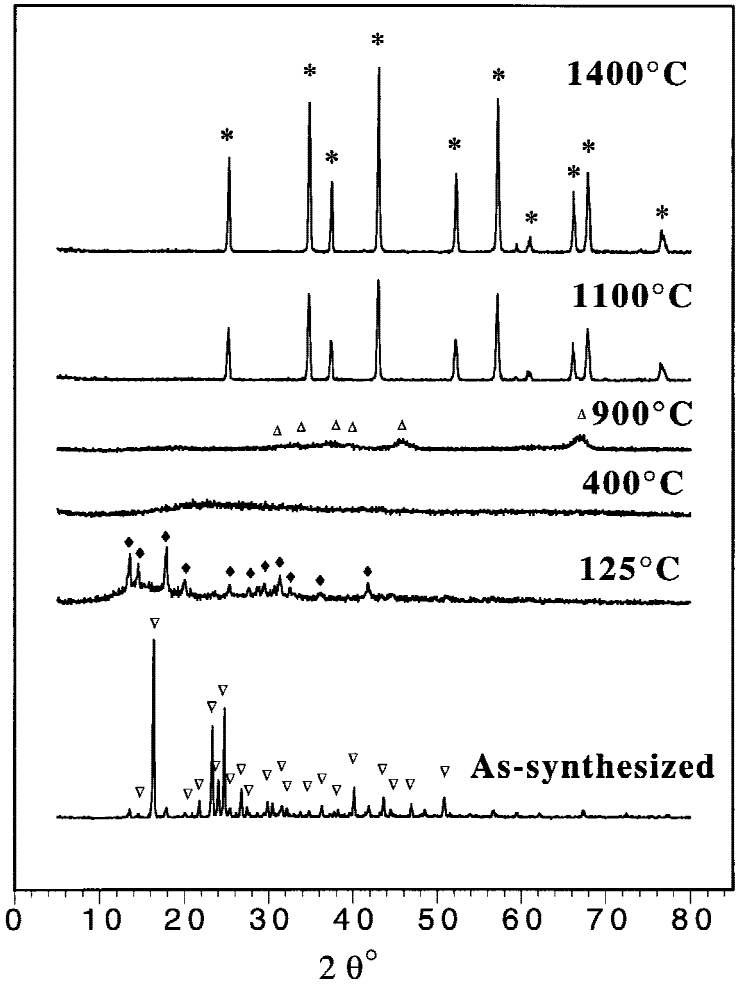

Fig. 4. XRD spectra of $Al(O_2CH)_3 \cdot 3H_2O$ pyrolyzed at selected temperatures; the samples were prepared as in DRIFTS studies ((*) α-Al_2O_3 phase (JCPDS File Card No. 10-173), (△) η-Al_2O_3 phase (JCPDS File Card No. 4-875), (♦) $Al(OH)(O_2CH)_2 \cdot xH_2O$ phase (JCPDS File Card No. 37-771), and (▽) $Al(O_2CH)_3 \cdot 3H_2O$ (Chaplygina *et al.*[31])).

$$YO(O_2CCH_3) \xrightarrow{\sim 400^\circ C} Y_2O_3 + Y_2(CO_3)_3 \text{ (minor)} + \text{gases } (CO_2, H_2O, (CH_3CO)_2O, \text{other}) \uparrow \quad (9)$$

The ceramic yield for this process would be ~62 wt%, whereas the observed ceramic yield from 265° to 340°C is ~56 wt%. This observation, coupled with the 300°C (2 h) DRIFTS spectrum (below), shows that the continued presence of ν(C−H) and carboxylate bands, albeit of decreased intensity, provide some support for a reaction akin to reaction (8) that occurs during the decomposition of $Y(O_2CCH_3)_3$.

Note that experimental differences between the TGA and DTA plots make the temperatures different for the same thermal event, although the TGA and DTA studies were performed

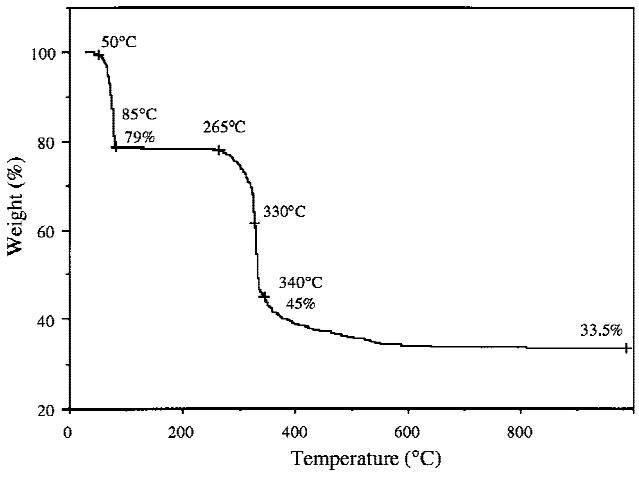

Fig. 5. TGA of $Y(O_2CCH_3)_3 \cdot 4H_2O$ in air.

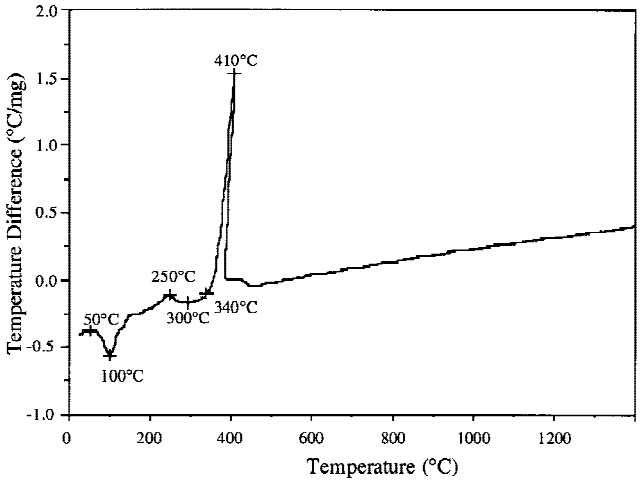

Fig. 6. DTA of $Y(O_2CCH_3)_3 \cdot 4H_2O$ in air; the sample was heated at the same heating rate as TGA for $Y(O_2CCH_3)_3 \cdot 4H_2O$ at temperatures <1000°C and then at 10°C/min to 1500°C at temperatures >1000°C.

at the same heating rate. In the DTA, the air flows (from below) past the sample pan; therefore, no fresh air flows directly on the sample, as in the TGA. Also, the DTA sample pan is deeper than the TGA pan and seems to form a dead-air zone; therefore, less sample surface is exposed to fresh air. Thus, the dead zone in the DTA inhibits decomposition, and these reactions have a tendency to start at higher temperatures. In our previous study on the pyrolysis behavior of $Y(O_2CCHMe_2)_3$, bcc Y_2O_3 crystallized at 300°C/2 h. An exotherm that was associated with crystallization was observed beginning at 280°C (maximized at 380°C.[1]

(B) DRIFTS: Figure 7 displays DRIFTS spectra for $Y(O_2CCH_3)_3{\cdot}4H_2O$ samples that have been pyrolyzed using the same procedures as those which were used for $Al(O_2CH)_3{\cdot}3H_2O$. The spectrum of $Y(O_2CCH_3)_3{\cdot}4H_2O$ (lowest inset in Fig. 7) shows weak ν(O−H) bands in the wave number range of 3500–2800 cm^{-1}, weak ν(C−H) bands at 3010, 2960, and 2950 cm^{-1}, and strong ν(C=O) bands at 1560, 1450, and 1350 cm^{-1}.[34]

As shown in the insets, when heated to 120° and then 300°C, the ν(C−H) band intensities diminish as $Y(O_2CCH_3)_3{\cdot}4H_2O$ seems to decompose to $YO(O_2CCH_3)$ or some related product. The continued presence of ν(O−H) bands may indicate a different product or the fact that the samples are prepared in air and DRIFTS emphasizes surface species (e.g., water that has been physisorbed during sample preparation). Most peaks at wave numbers <1750 cm^{-1} remain unchanged, as also observed by Hussein.[34] However, a weak ν(Y−O) band at 560 cm^{-1} suggests the presence of Y_2O_3.[1,36] The 560 cm^{-1} peak grows in intensity at higher temperatures. In the $Y(O_2CCHMe_2)_3$ pyrolysis studies, where bcc Y_2O_3 forms at 300°C/2 h, DRIFTS peaks that correspond to crystalline Y_2O_3 appeared simultaneously at 560, 470, and 430 cm^{-1}.[1,34] In the current study, the 300°C/2 h pyrolyzed $Y(O_2CCH_3)_3{\cdot}4H_2O$ sample likely consists of a mixture of Y_2O_3 and $YO(O_2CCH_3)$. It is also possible that some carbonate forms; however, the carbonate bands would be hidden beneath the ν(C=O) bands.

At 500°C (DRIFTS spectrum not shown), the ν(C=O) bands disappear, and carbonate peaks appear at 1530 and 1405 cm^{-1}, which suggests the formation of $Y_2(CO_3)_3$. The 600°C spectrum is quite similar to the 500°C spectrum, except for a decrease in the carbonate peak intensities. These peaks finally disappear at 800°C, which indicates the complete elimination of carbonate. Indeed, most of the carbonate is gone by 600°C; only an additional 2 wt% loss is observed. The remaining material is assumed to be stoichiometric Y_2O_3. The intensities of the peaks at 560, 470, and 430 cm^{-1} increase as the temperature increases from 500°C to 1400°C, which indicates continued crystallization and/or grain growth of Y_2O_3, as supported by XRD studies. Again, all the intermediate pyrolysis samples were white powders.

(C) Powder X-ray Diffractometry (XRD) Patterns: Figure 8 displays powder XRD patterns for $Y(O_2CCH_3)_3{\cdot}4H_2O$ pyrolysis samples that were produced as in the DRIFTS studies. The XRD pattern for the as-recrystallized sample is similar to that of Hussein.[34] Although there is no significant change in the DRIFTS spectrum for the sample pyrolyzed to 300°C, the XRD data for the recrystallized samples pyrolyzed to 120° and 300°C are quite different, which suggests structural changes when heated. Although Hussein[34] suggested that crystalline

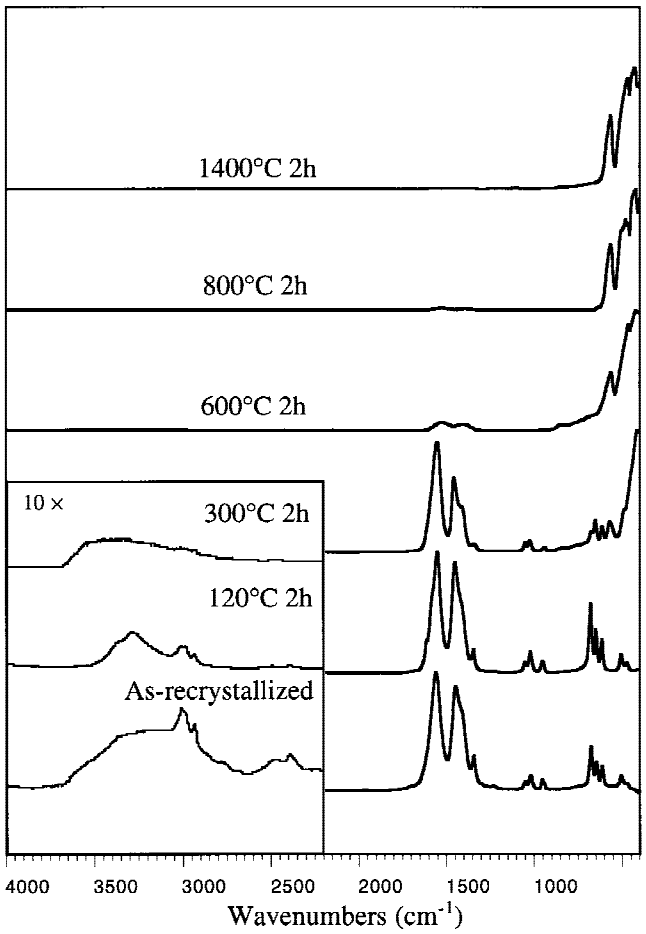

Fig. 7. DRIFTS spectra of $Y(O_2CCH_3)_3{\cdot}4H_2O$ pyrolyzed at 10°C/min (2 h dwell) in air at the selected temperatures.

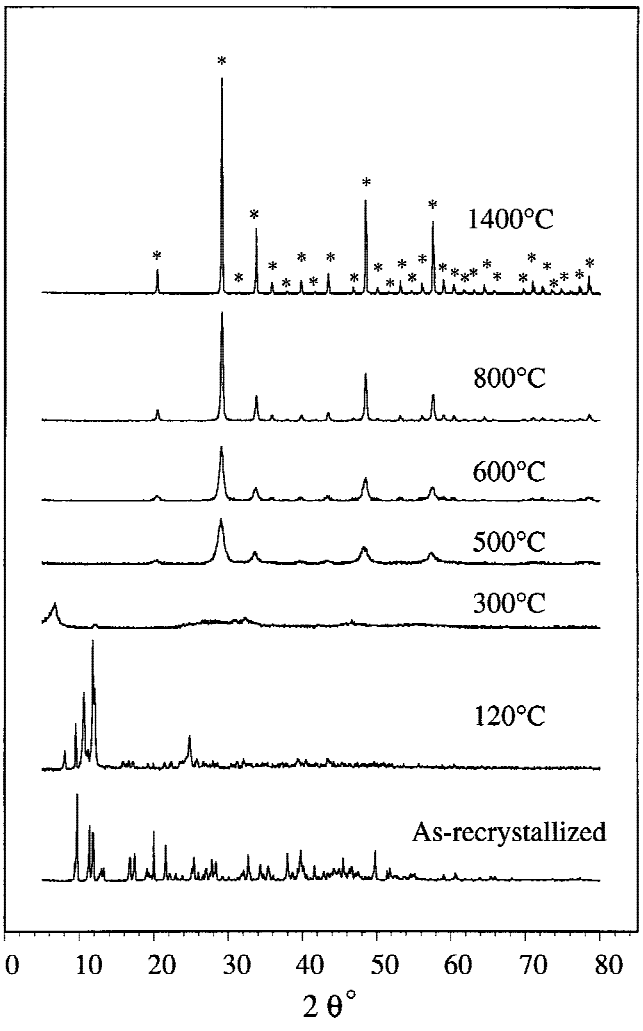

Fig. 8. XRD spectra of $Y(O_2CCH_3)_3{\cdot}4H_2O$ pyrolyzed at selected temperatures; the samples were prepared as in DRIFTS studies ((*) bcc yttria (JCPDS File Card No. 41-1105)).

$Y(O_2CCH_3)_3$ is stable to 350°C/1 h, our XRD data indicate the formation of a new, intermediate crystalline or partially crystalline phase at 300°C/2 h. This phase may correspond to ''$YO(O_2CCH_3)$,'' which is suggested by the TGA, DTA, and DRIFTS evidence and the work on the aluminum analogue.[35] However, no further evidence is available to support this explanation.

At 500°C, the XRD pattern shows crystalline bcc Y_2O_3; however, the broad peaks and low intensities suggest that considerable material is either amorphous or nanocrystalline, as observed in the XRD profile for $Y(O_2CiPr)_3$ at 300°C.[1] It is possible that the presence of carbonate inhibits crystallization; however, no evidence supports this conjecture. At higher temperatures (≥600°C), the XRD intensities increase and the peak widths narrow, which indicates better crystallization. At 1400°C, the XRD profile indicates well-crystallized Y_2O_3.

(4) Characterization of $3Y(O_2CCH_3)_3$:$5Al(O_2CH)_3$ YAG Precursor Mixture

The YAG precursor was prepared by dissolution of the correct stoichiometric mixture in H_2O, formic acid, isobutyric acid, and ethylene glycol, followed by vacuum evaporation of the solvent and grinding of the resulting powder, as detailed in the experimental section. Samples of this bulk powder were then pyrolyzed to selected temperatures as discussed previously.

(A) Thermal Analysis: The TGA plot of the bulk, dry (100°C/2 h) powder (Fig. 9) seems to show a decomposition profile that is not a simple superposition of both $Al(O_2CH)_3 \cdot 3H_2O$ and $Y(O_2CCH_3)_3 \cdot 4H_2O$ decomposition profiles. There are five mass-loss steps during decomposition, according to the derivative curve. The first one, beginning at 120°C (mass loss of 10 wt%), corresponds to the elimination of water and loosely bound organics. The second one, from 180°C (centered at 210°C, mass loss of 8 wt%), corresponds to the partial decomposition of carboxylate ligands, possibly via reactions (3) and (8). The third mass loss, from 240°C (centered at 310°C, mass loss of 30 wt%), probably corresponds to the decomposition of the residual carboxylate ligands, as ν(C−H) bands disappear (see DRIFTS section) and the color of the sample changes from white to light brown. The fourth loss, from 400°C to 920°C (mass loss of 9 wt%), is associated with carbonate decomposition. The sample coincidently becomes black at temperatures >600°C. The fifth loss, from 930° to 1000°C (mass loss of 3 wt%), results from the oxidation of trace amounts of free carbon, as samples change from black to white. The presence of residual carbon at such high temperatures, in an oxidizing atmosphere, is not commonly observed for the pyrolytic decomposition of aluminosilicates, nor was such behavior noted in the isobutyrate studies.[14]

The found ceramic yield is 40.0 wt%, whereas a ceramic yield of 28.3 wt% is calculated for $3[Y(O_2CCH_3)_3 \cdot 4H_2O] \cdot 5[Al(O_2CH)_3 \cdot 3H_2O]$. The calculated ceramic yield for anhydrous $3[Y(O_2CCH_3)_3] \cdot 5[Al(O_2CH)_3]$ is 36.9 wt%, which is also lower than the found value. It is possible that some $Al(O_2CH)_3 \cdot 3H_2O$ transforms to $Al(OH)(O_2CH)_2$ when the YAG precursor is vacuum dried at 100°C. The calculated ceramic yield for $3[Y(O_2CCH_3)_3] \cdot 5[Al(OH)(O_2CH)_2]$ is 40.4 wt%, which is similar to the TGA ceramic yield. However, the DRIFTS data do not show the presence of ν(O−H). Alternately, the precursor is actually $3[Y(O_2CH)_3] \cdot 5[Al(O_2CH)_3]$, which offers a ceramic yield of 40.1 wt%, which also is similar to that found. The acetate ligands may exchange with the free HCO_2H that has been used as a stabilizer during precursor synthesis.

In Fig. 10, the DTA shows three exotherms at temperatures <900°C. The first one, which is centered at 230°C, likely corresponds to the second mass loss step in the TGA and may be associated with the partial decomposition of formate to $M(OH)(O_2CH)_2$ (M = Al and/or Y) species (see DRIFTS, section III*(4)(B)*). The second exotherm, which is centered at 340°C (third mass loss step in TGA, 260°–420°C), corresponds to a mass loss of ~30 wt% in TGA. In this temperature range, the carboxylate ligands decompose primarily to carbonate and oxide species (see DRIFTS, section III*(4)(B)*). The third exotherm, which is centered at 440°C (fourth step in the TGA, mass loss of ~3 wt%), likely corresponds to the oxidation of residual organics and network formation.[14] However, the black color of the materials clearly indicates the presence of some residual carbon.

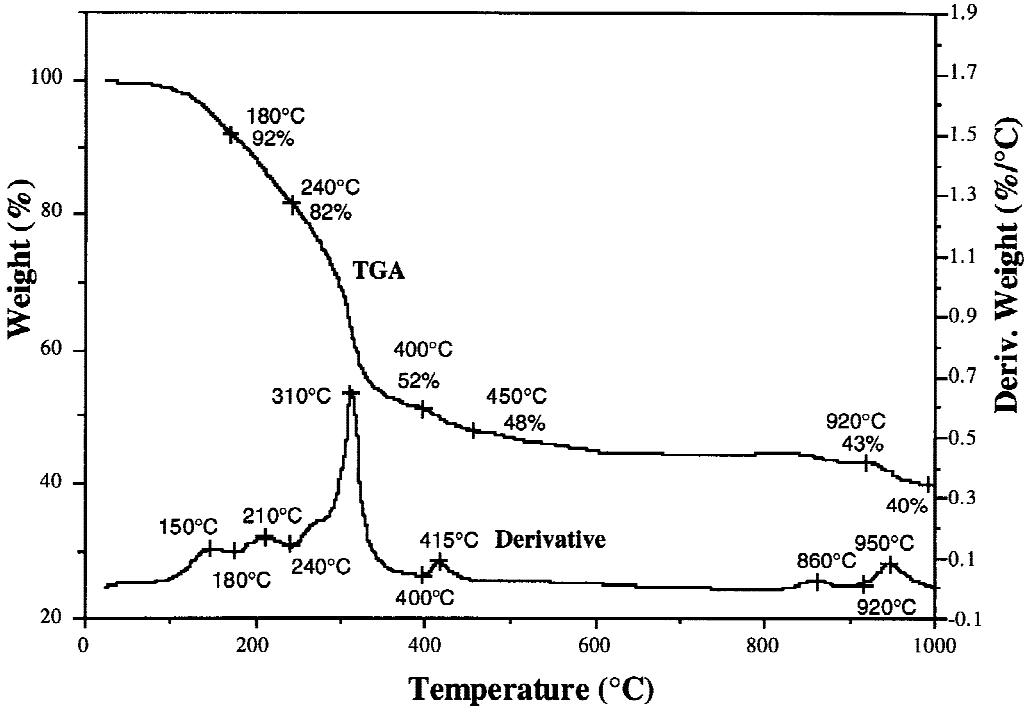

Fig. 9. TGA of YAG formate/acetate precursor in air.

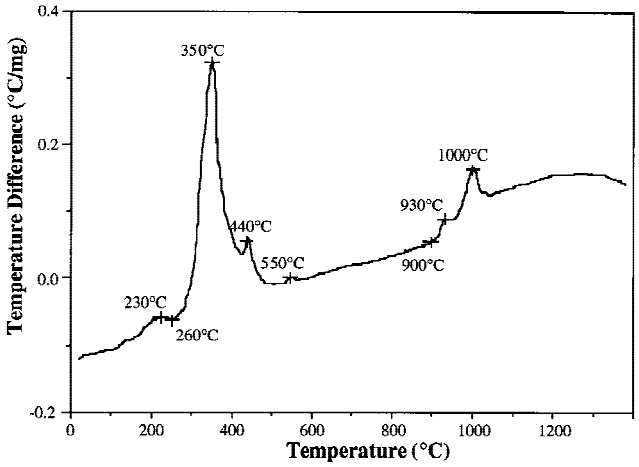

Fig. 10. DTA of YAG formate/acetate precursor in air.

None of the DTA peaks has a common position with the DTA studies of the individual aluminum and yttrium compounds (Figs. 2 and 6). Such behavior implies that the YAG precursor is not simply a mechanical mixture of the individual aluminum and yttrium compounds. For example, the YAG precursor that has been pyrolyzed at 600°–800°C/2 h is black, although neither the aluminum nor the yttrium carboxylates generate black pyrolysis products. We have previously observed similar synergistic behavior following THF dissolution and recovery of mixtures of Cu/Ba and Y/Al isobutyrates.[1,7]

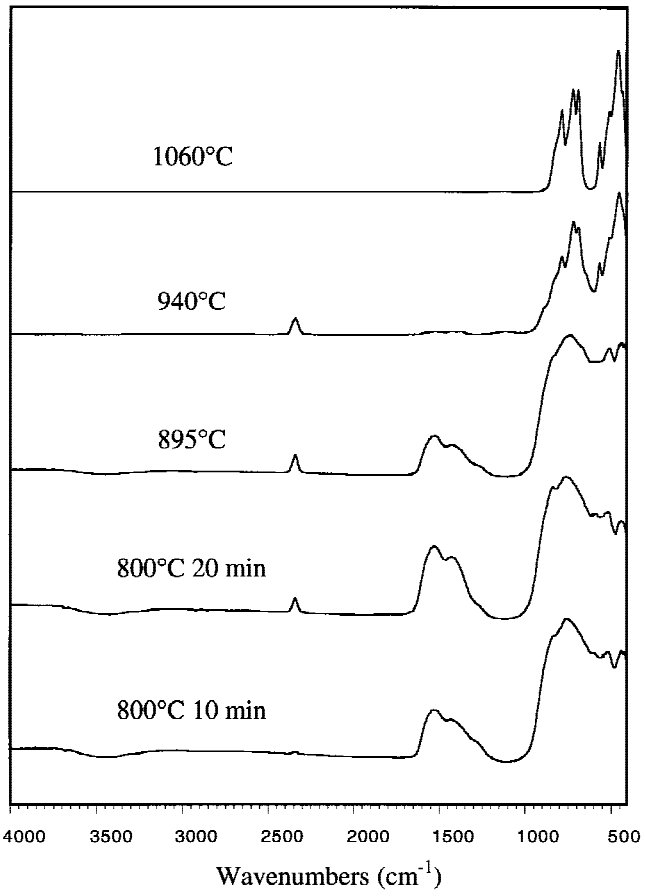

Fig. 11. DRIFTS spectra of DTA-pyrolyzed YAG formate/acetate precursor; the samples were heated at 10°C/min to the selected temperature, with a holding time of ~1 s for 895°, 940°, and 1060°C.

One possible interpretation is that a mixed-metal carboxylate complex is forming; however, we have not sought to explore this possibility.

The DTA (Fig. 10) also shows two exotherms, at 930° and 1000°C (fifth step in the TGA). Because we were concerned about the origin of both peaks, an additional DRIFTS study was conducted with the DTA samples. A series of DRIFTS spectra were taken between the two exotherms, to follow the evolution of the precursor (Fig. 11). The YAG precursor powder remained black until just above 890°C, which is the temperature below the onset point of the first exotherm. At 895°C (no dwell time), the sample displayed broad carbonate peaks with reasonably strong intensities, as does the 400°C/2 h amorphous sample in Fig. 12. Between 930° and 1000°C, the sample was gray. The DRIFTS analysis for a sample that has been heated at 940°C (no dwell time) shows a typical crystalline YAG profile, with the carbonate peaks absent (Fig. 11). At 1060°C, where the second exotherm is complete, the sample was white. The DRIFTS analysis for the sample that has been held at 1060°C (no dwell time) is almost the same as the DRIFTS analysis for the 940°C sample, which suggests no changes at the atomic level. Based on the above-mentioned observations, one can conclude that the first exotherm results from the oxidation of carbon and the second results from the crystallization of YAG.

(B) DRIFTS: Figure 12 displays spectra of the as-processed YAG precursor and samples that have been heated to selected temperatures. The as-processed YAG precursor spectrum (bottom) is similar to that of $Al(O_2CH)_3 \cdot 3H_2O$ but with broader peaks. It is possible that the $Y(O_2CCH_3)_3 \cdot 4H_2O$ peaks are hidden by $Al(O_2CH)_3 \cdot 3H_2O$ peaks, because of the higher concentration of the aluminum compound, or a new mixed-metal complex forms. Alternately, based on the changes in ceramic yield, the acetate ligands may have been displaced by formate ligands during synthesis of the YAG precursor.

At 250°C, the major peak positions do not change; however,

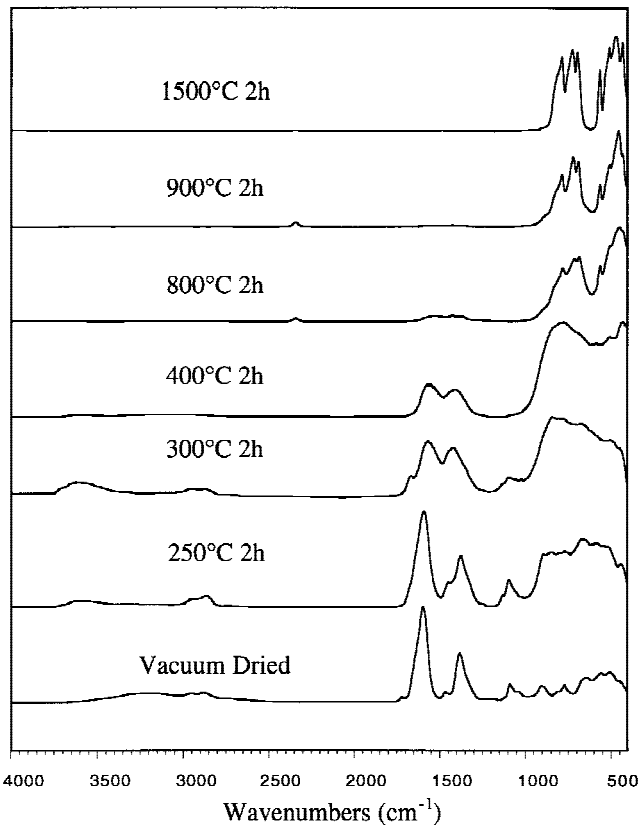

Fig. 12. DRIFTS spectra of YAG formate/acetate precursor heated at 10°C/min to selected temperatures, followed by a holding time of 2 h.

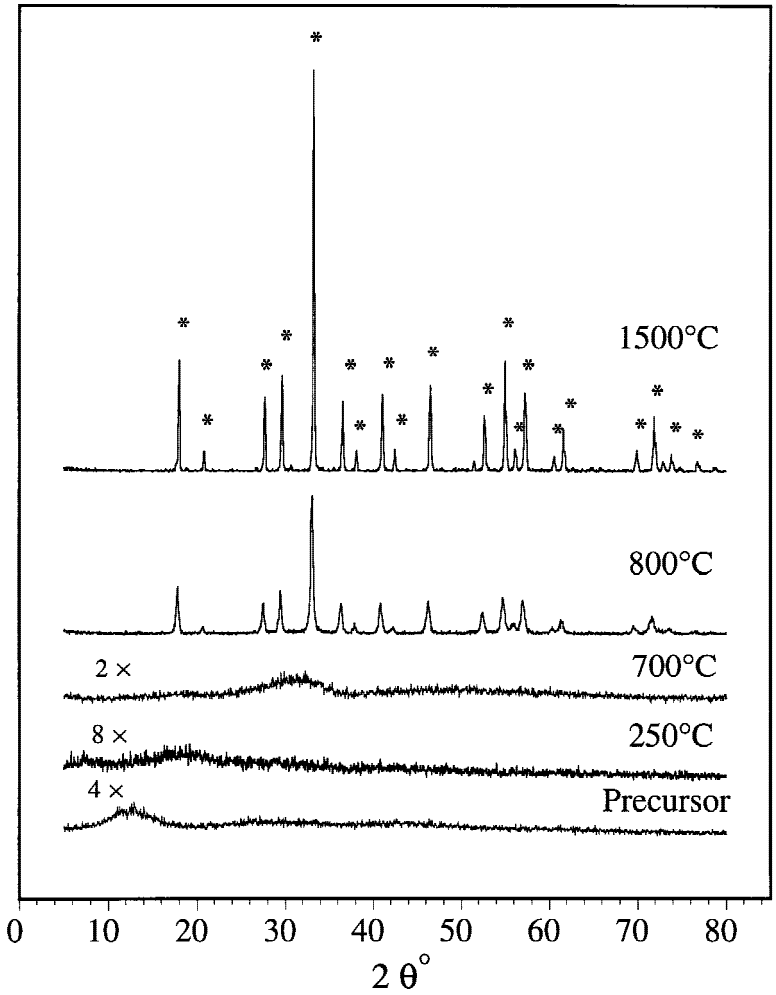

Fig. 13. XRD spectra of YAG formate/acetate precursor pyrolyzed to selected temperatures; the samples were treated as in DRIFTS studies ((*) YAG (JCPDS File Card No. 33-40)).

the broad ν(OH) band at 3600–3200 cm^{-1} (hydrate water) disappears and a ν(OH) band appears at 3700–3400 cm^{-1} that can be assigned to O−H stretches of Al/Y hydroxyl groups, which suggests partial hydrolytic decomposition (e.g., reaction (3)).

At 300°C, the ν(C = O) bands at 1600, 1464, and 1380 cm^{-1} disappear and carbonate peaks that are centered at 1530 and 1400 cm^{-1} appear. The ν(C−H) bands at 2950 and 2880 cm^{-1}, and the ν(O−H) band at 3700–3400 cm^{-1} are still observed in the spectrum, which suggests that carboxylate ligand decomposition is incomplete.

At 400°C, all bands that are associated with the carboxylate ligands disappear (in the YAG isobutyrate precursor study, the carboxylate ligands disappear at 300°C).[1] Two broad carbonate peaks centered at 1530 and 1400 cm^{-1} appear. All the remaining peaks are broad as well, which indicates an amorphous material.

The carbonate peaks persist to only 800°C (note 2 h dwell versus no dwell in Fig. 11), as observed for the isobutyrate precursor.[1] The broad peaks at 650–1000 cm^{-1} in the 300°–400°C spectra evolve into a set of peaks at temperatures ≥800°C that correspond to the crystallization of YAG.[1,37]

(C) XRD: Figure 13 provides XRD powder patterns of bulk YAG precursor samples that have been pyrolyzed to selected temperatures. As with the YAG isobutyrate studies,[1] no intermediate crystalline phases (e.g., bcc Y_2O_3, η- or α-Al_2O_3) are observed before the crystallization of YAG (~800°C). Formate/acetate-derived YAG crystallizes at temperatures that are ~100°C lower than the isobutyrate precursor.[1]

The dried precursor exhibits broad peaks centered at 12° 2θ, which is typical of an amorphous material. When the precursor is heated to 700°C, this peak shifts to 30° 2θ, which indicates a change in the amorphous structure, perhaps suggesting some local ordering, as implied by the peaks at 650–1000 cm^{-1} in the DRIFTS spectra at the same temperature. This type of behavior

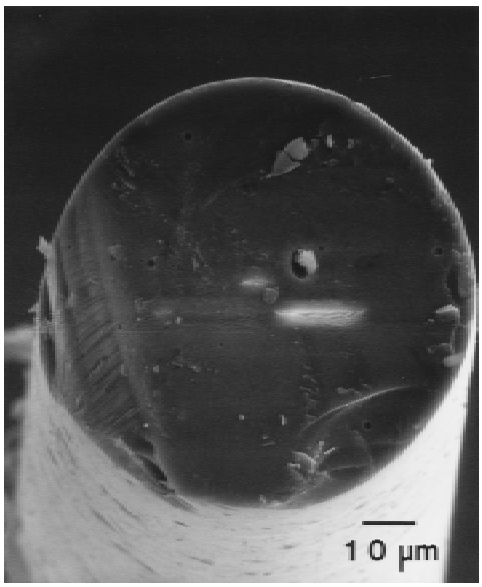

Fig. 14. SEM micrograph of as-spun extruded YAG isobutyrate precursor fiber.

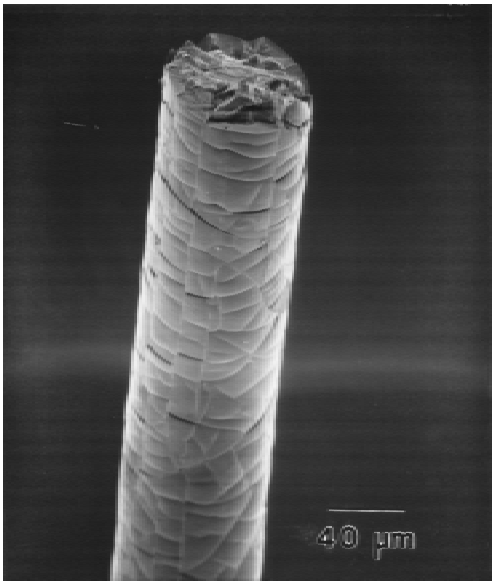

Fig. 15. SEM micrograph of extruded isobutyrate precursor fiber cured at 1°C/min to 160°C (dwell time of 2 h).

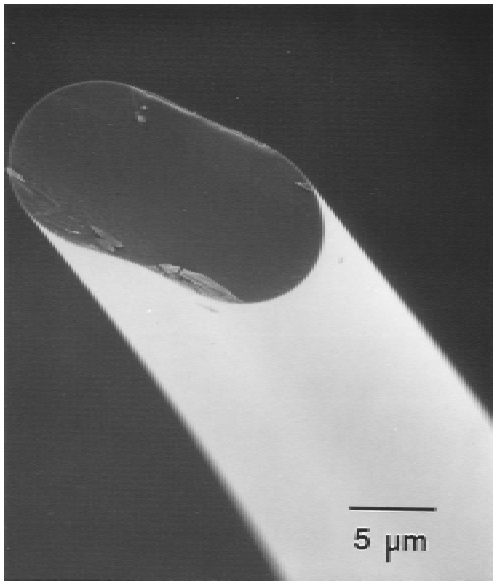

Fig. 17. SEM micrograph of as-spun extruded YAG formate/acetate precursor fiber.

has been termed ''noncrystalline but not completely amorphous.''[1,13]

The appearance of crystalline YAG at temperatures that are ~100°C lower than YAG from the isobutyrate precursor may suggest better atomic mixing, a lower stability precursor, or better nucleation of crystallites during decomposition, because of a higher impurity level. The exact reasons for this behavior cannot be explained at present.

At temperatures >800°C, YAG continues to crystallize, as evidenced by the continued refinement in peak shapes and intensities. The difference in phase-transformation temperatures between the DTA and IR/XRD analyses is due to differences in the heating schedule, because crystallization of YAG at 800°C is not only temperature dependent, but also is atmosphere and time dependent. The IR/XRD samples were heat treated at selected temperatures for 2 h, whereas the DTA data were obtained for samples that were heated continuously to 1500°C. A longer heating time, at lower temperatures, generates the same phase changes in the bulk IR/XRD samples, as observed for the higher-temperature, shorter-time transformations in the DTA. Thus, the exothermic crystallization peak in the DTA occurs at ~1000°C rather than the 800°C crystallization temperature that has been observed in the XRD studies. Crystallization occurs coincident with the elimination of carbon.

Samples that have been pyrolyzed at 800°C/1 h/air are black, and the XRD and DRIFTS analyses both indicate an amorphous material. A sample that has been held for 2 h at 800°C is mostly white, and XRD and DRIFTS analyses reveal crystalline YAG. In the DTA, the air flow is toward the bottom of the sample pan, therefore, no fresh air flows toward the sample directly, and the temperature is ramped continuously, rather than dwelling at a selected temperature for 2 h. Thus, the DTA sample at 895°C is still black and amorphous. When the sample is heated further, free carbon is oxidized and eliminated as CO_2, and phase transformation occurs. Thus, atmosphere has a

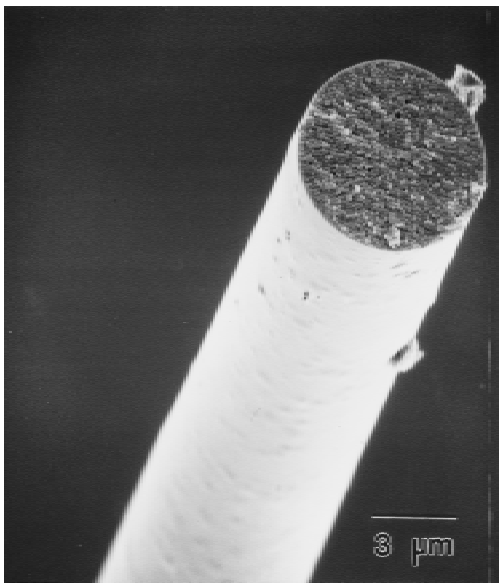

Fig. 16. SEM micrograph of hand-drawn isobutyrate fiber heated to 1000°C for 2 h.

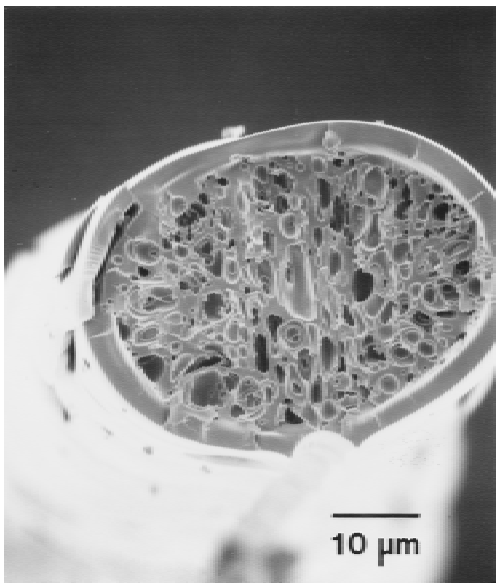

Fig. 18. SEM micrograph of extruded YAG formate/acetate fiber heated at 1°C/min to 100°C for 2 h, then to 700°C for 2 h.

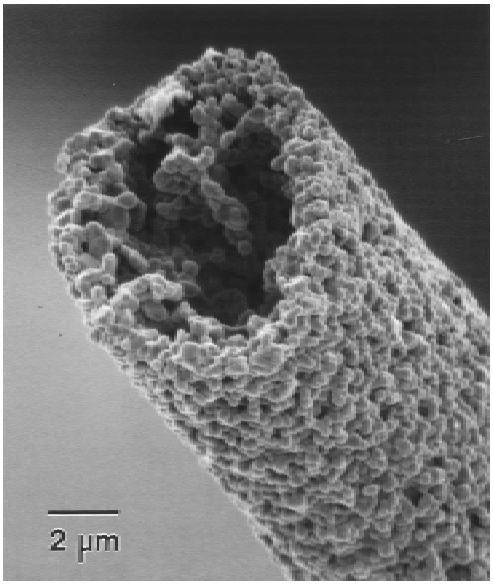

Fig. 19. SEM micrograph of extruded YAG formate/acetate fiber heated at 1°C/min to 100°C for 2 h, then at 20°C/min to 1500°C for 2 h.

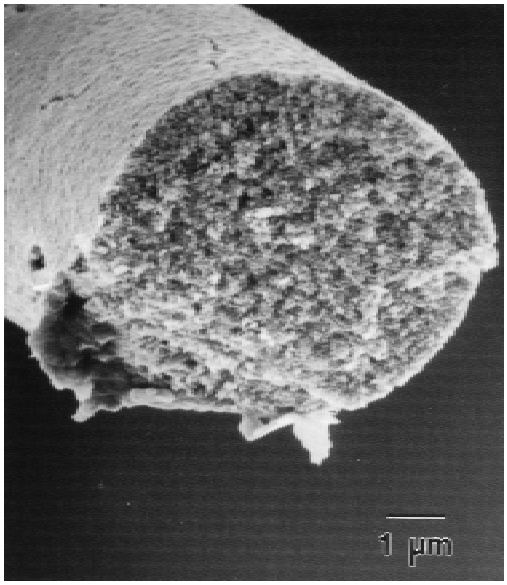

Fig. 21. SEM micrograph of extruded YAG formate/acetate precursor fiber heated at 1°C/min to 100°C for 2 h, 1°C/min to 400°C for 2 h, and then 15°C/min to 900°C for 2 h.

role in crystallization, because the carbon impurities seem to retard crystallization.

(D) Fiber Processing: To successfully process fully dense, defect-free, polycrystalline YAG fibers, the experimental design must allow for the extreme changes in volume and density that occur as the green precursor fiber transforms to a ceramic fiber. The first step is to clearly define the conditions under which these changes occur by doing bulk material studies. These studies provide an idea of the time/temperature dependence on YAG evolution from precursor and permit the design of a heat-treatment schedule to process dense, carbon-free YAG fibers.

(E) Al/Y Isobutyrate YAG Precursor Fiber Processing: Based on our earlier studies of the Al/Y isobutyrate YAG precursor,[1] YAG isobutyrate precursor fibers were processed by hand drawing and extrusion, followed by pyrolysis. Figure 14 shows an SEM micrograph of an extruded green isobutyrate fiber. The as-processed green fiber has a circular cross section, a smooth surface, and is 70 μm in diameter. When the sample is heated to 160°C, cracks form (Fig. 15). A likely explanation for cracking is that the fiber diameters are too large; thus, the gas diffusion distances are too long. Consequently, gaseous decomposition products accumulate at the subsurface level to form gas bubbles that damage the fibers. For example, a 20 mg precursor (17.5 mm^3) releases 2 mg of gaseous byproducts at 200°C (the TGA in Fig. 9 shows a 10% mass loss at 200°C). If the gaseous byproducts are assumed to be either H_2O or CO_2, the generated volume (at room temperature) would be 4.3×10^3 mm^3 (for H_2O) or 1.8×10^3 mm^3 (for CO_2). Each volume is a factor of >100 greater than the volume of the precursor material.

Based on this consideration, thinner fibers (green-fiber di-

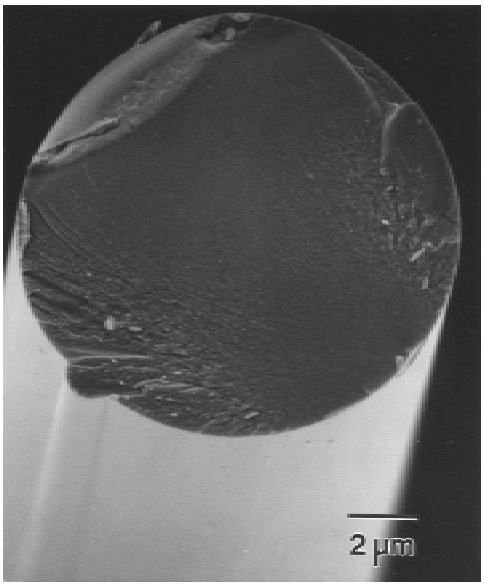

Fig. 20. SEM micrograph of extruded YAG formate/acetate precursor fiber heated at 1°C/min to 110°C for 2 h and then 1°C/min to 400°C for 2 h.

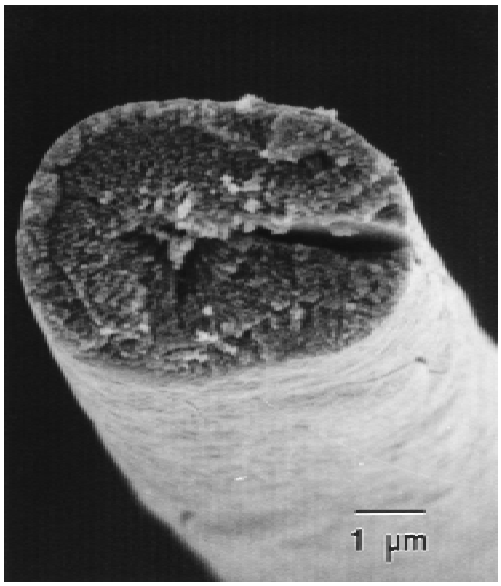

Fig. 22. SEM micrograph of extruded YAG formate/acetate precursor fiber heated at 1°C/min to 100°C for 2 h, 1°C/min to 400°C for 2 h, and then 15°C/min to 1000°C for 2 h.

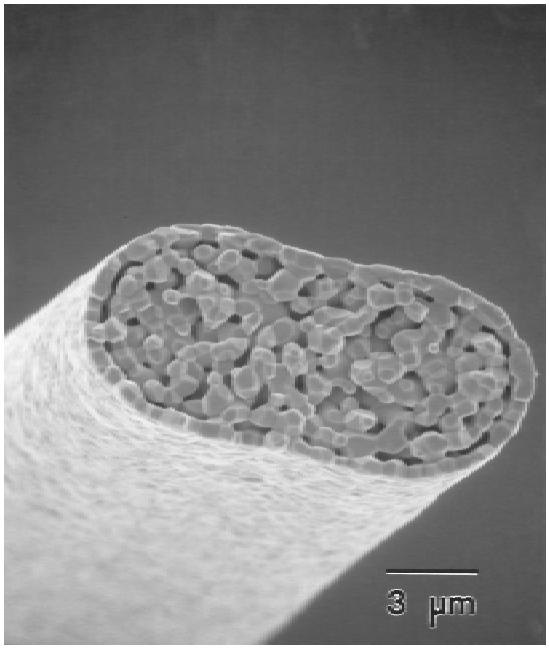

Fig. 23. SEM micrograph of extruded YAG formate/acetate precursor fiber heated at 1°C/min to 100°C for 2 h, 1°C/min to 400°C for 2 h, 15°C/min to 900°C for 2 h, and then 15°C/min to 1570°C for 2 h.

ameters of <20 μm) with shorter diffusion distances were made by hand drawing. Thin, crack-free but somewhat porous YAG fibers were obtained by heating to 1000°C in air (Fig. 16). Although the fibers are not fully dense, they may still offer useful properties, because their internal porosity is reminiscent of that observed for FP alumina (DuPont, Wilmington, DE) fibers.[7,16,38,39]

(5) Fibers from $Al(O_2CH)_3 \cdot 3H_2O$ and $Y(O_2CCH_3)_3 \cdot 4H_2O$

(A) Density and Volume Changes: The measured density for the YAG precursor is 1.5 g/cm^3, whereas the reported density of YAG is 4.5 g/cm^3. Thus, the theoretical volume change that results from both mass loss and densification is 87%. If we assume that the volume changes that occur as a precursor fiber is pyrolyzed occur only in the diametrical dimension and that full densification results, the expected change in fiber diameter will be 64%. These extensive volume changes must be carefully controlled to ensure that uniform, stress-free ceramic fibers result following pyrolysis.

(B) Green Fiber Processing: As discussed previously, the size (diameter) of the green fiber (Fig. 17) is important to process dense, defect-free YAG fibers. Large-diameter (>30 μm) green fibers foam or crack during decomposition (e.g., the 40 μm diameter fiber in Fig. 18, which was pyrolyzed to 700°C/2 h). The optimum size is <30 μm, preferably <20 μm (e.g., as shown in Fig. 17). These acetate formate fibers are easily extruded to give green fibers that are 20 μm in diameter and look similar to that shown in Fig. 14. Although the spinneret orifice (~80 μm) is circular, extruded green fibers often have a dog-bone cross section, because of uneven drying. Green fibers that have been dried under tension have circular cross sections.

(6) Fiber Pyrolysis

(A) Low-Temperature Pyrolysis: All fibers were heated at 100°C/2 h to remove solvent, water of hydration, and processing aids. Fine green fibers (diameters of ~10 μm) that were pyrolyzed at a rate of 20°C/min directly to 1500°C/2 h were porous (Fig. 19). Two factors contribute to the observed porosity. First, with fast heating rates, the surface material decomposes first, which eliminates surface carbonate, and densification/crystallization occurs first at the surface. The interior then gasifies, the pressure builds up, and cracks/flaws form as this gas evolves, which leads to hollow fibers. Second, the fibers do not densify coincident with ligand decomposition. To solve this problem, the fibers were heated at a rate of 1°C/min to 400°C/2 h, the temperature at which most carboxylates decompose. In this way, the gaseous byproducts diffuse out of the fibers slowly and completely. Fibers that were processed with this heat treatment were dense (see Fig. 20). Consequently, as organics and carbonate in the fiber center decompose, the gaseous byproducts cannot diffuse easily out of the fibers and some voids/internal pores form. To solve this problem, a relatively low heating rate, 10°C/min, was selected, and holding

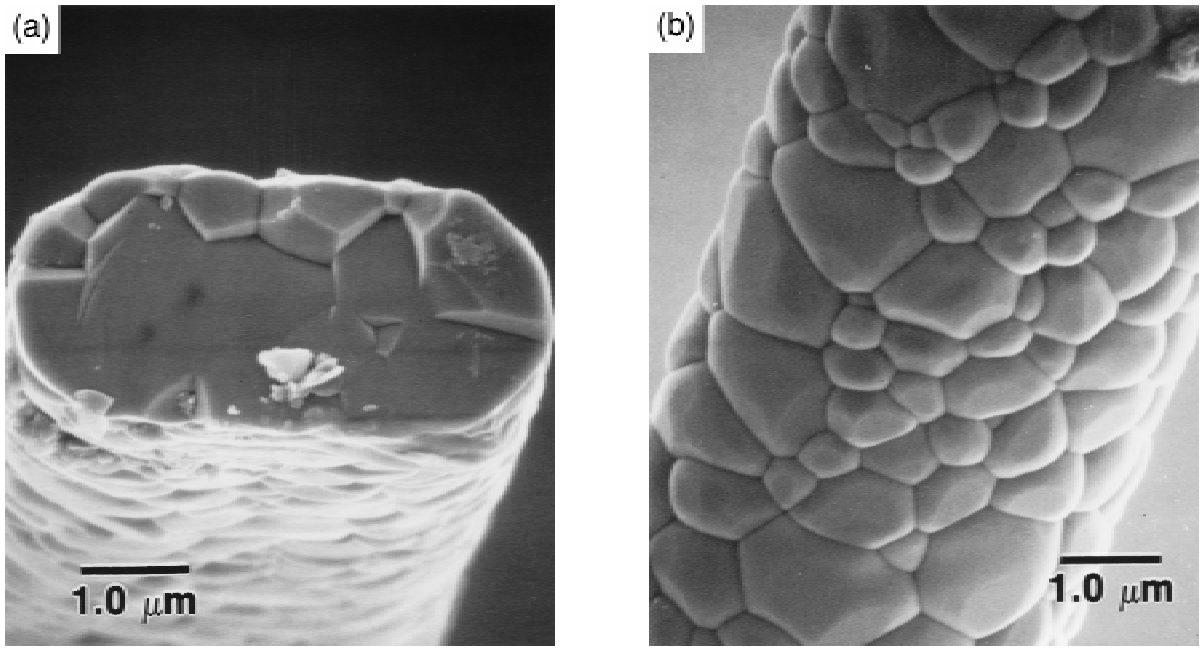

Fig. 24. SEM micrographs of extruded YAG formate/acetate precursor fiber heated at 1°C/min to 100°C for 2 h, 1°C/min to 400°C for 2 h, 15°C/min to 900°C for 2 h, and then 30°C/min to 1570°C for 2 h.

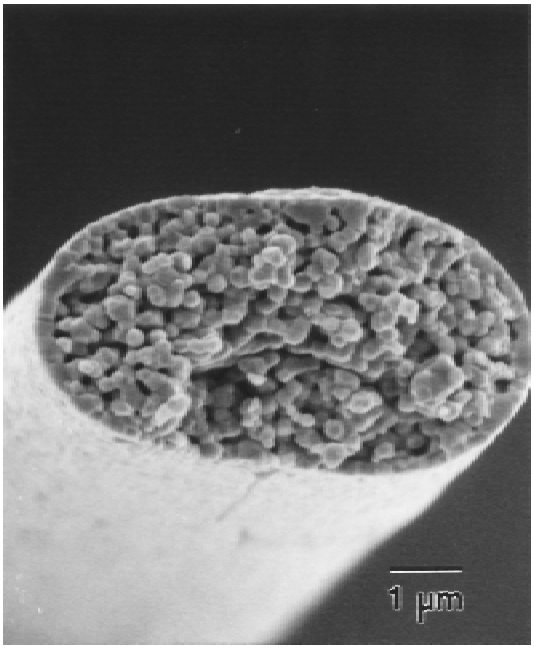

Fig. 25. SEM micrograph of extruded YAG formate/acetate precursor fiber heated at 1°C/min to 100°C for 2 h, 1°C/min to 400°C for 2 h, 15°C/min to 900°C for 2 h, and then 30°C/min to 1400°C for 2 h.

periods of 2 h at temperatures of 900° or 1000°C were used to cautiously eliminate carbonate. At these temperatures, YAG grains do not grow dramatically and the fiber surface does not completely densify, as shown in Figs. 21 and 22.

(B) Heating-Rate Studies: Post pyrolysis studies (after heat treatment at 900°C) were conducted to optimize densification and grain growth. Faster heating rates usually result in denser fibers.[10a] For example, 900°C fibers that have been heated at a rate of 15°C/min to 1570°C for 2 h are usually porous (Fig. 23), whereas those that have been heated at a rate of 30°C/min to the same temperature are dense (Fig. 24). In addition, a skin seems to form in the fiber shown in Fig. 23. A reasonable explanation is that the low heating rate that has been used still promotes more-efficient loss of impurities at the surfaces than in the interior, which results in faster pore coalescence and sintering at the surface than in the interior.

(C) Densification-Temperature Studies: Densification of 900°C fibers occurs at >1400°C. Figures 25–27 shows SEM micrographs of the 900°C fiber that has been ramped at a rate of 30°C/min to 1400°, 1500°, or 1600°C for 2 h. Fibers that have been sintered at 1400°C for 2 h exhibit porous cross sections (see Fig. 25). Fibers that have been sintered at 1500°C for 2 h are much denser (Fig. 26), although some voids form at the grain boundaries. Fibers that have been sintered at 1570° and 1600°C for 2 h are almost fully dense (Figs. 24 and 27).

(D) Mechanical Properties of YAG Fibers: Room-temperature fiber strength was characterized using a bending test.[28,29] The bend strength of 900°C fibers that have been sintered using post-pyrolysis heat treatments at rates of 30°C/min to 1570°, 1600°, or 1650°C for 2 h were assessed, as described in the experimental section. At least five fibers were tested for each heating schedule. SEM analysis shows fiber cross sections that are fully dense. For example, the fiber in Fig. 28 (1570°C/2 h) has a bend strength of 1.3 ± 0.3 GPa. This calculation is based on the assumption that the fibers that are tested are fully dense, have the same density as bulk material, and have the same elastic modulus (280 GPa)[28] as bulk material. Figure 29 provides a view of bend strength versus sintering temperature. Based on the results, a 1600°C sintering temperature offers the best strength, 1.7 ± 0.2 GPa, with an average grain size of 1.8 ± 0.2 μm (grain sizes were based on point-fraction analysis of SEM micrographs, and at least five fibers were measured for each heating schedule).

When the sintering temperature is >1600°C, the grain size increases and reduces the grain-boundary area (Fig. 30), thus reducing the room-temperature strength. Figure 31 plots the bend strength versus the grain size. From the limited amount of data, an average grain size of 1.8 μm seems to offer the best strength.

As discussed in the introduction, smaller grain sizes should provide better room-temperature strength if Hall–Petch-type criteria are valid; however, the 1570°C fibers with an average grain size of 1.2 μm have lower strength. Presently, we cannot explain why 1570°C sintering offers lower strength. One pos-

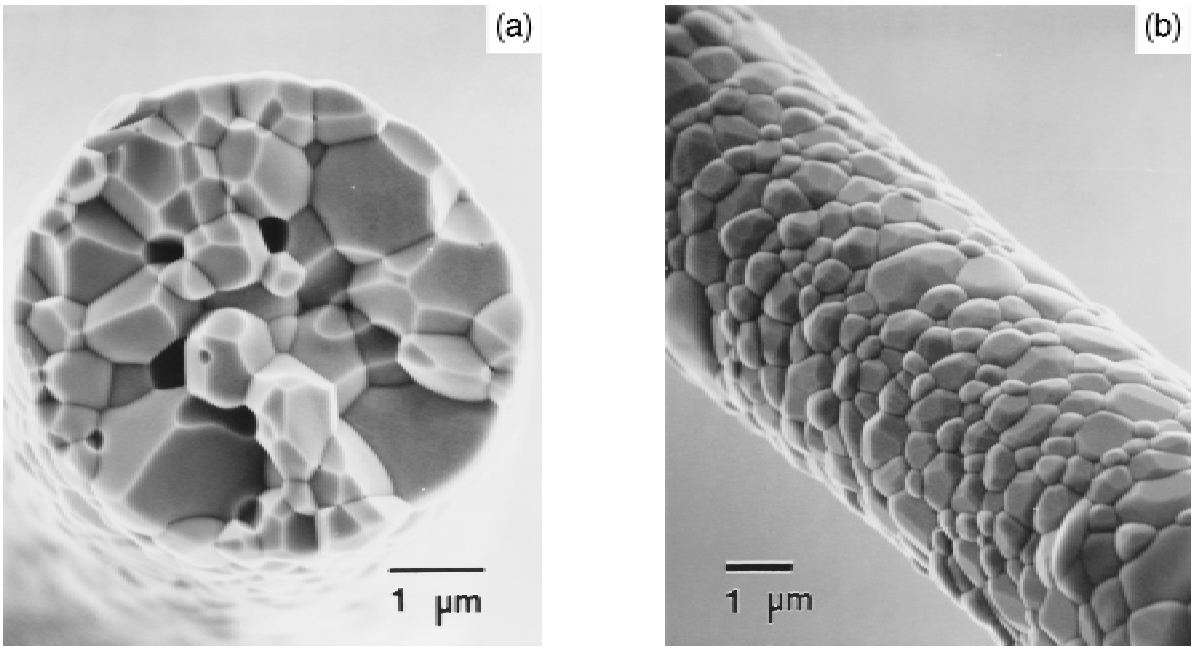

Fig. 26. SEM micrographs of extruded YAG formate/acetate precursor fiber heated at 1°C/min to 100°C for 2 h, 1°C/min to 400°C for 2 h, 15°C/min to 900°C for 2 h, and then 30°C/min to 1500°C for 2 h.

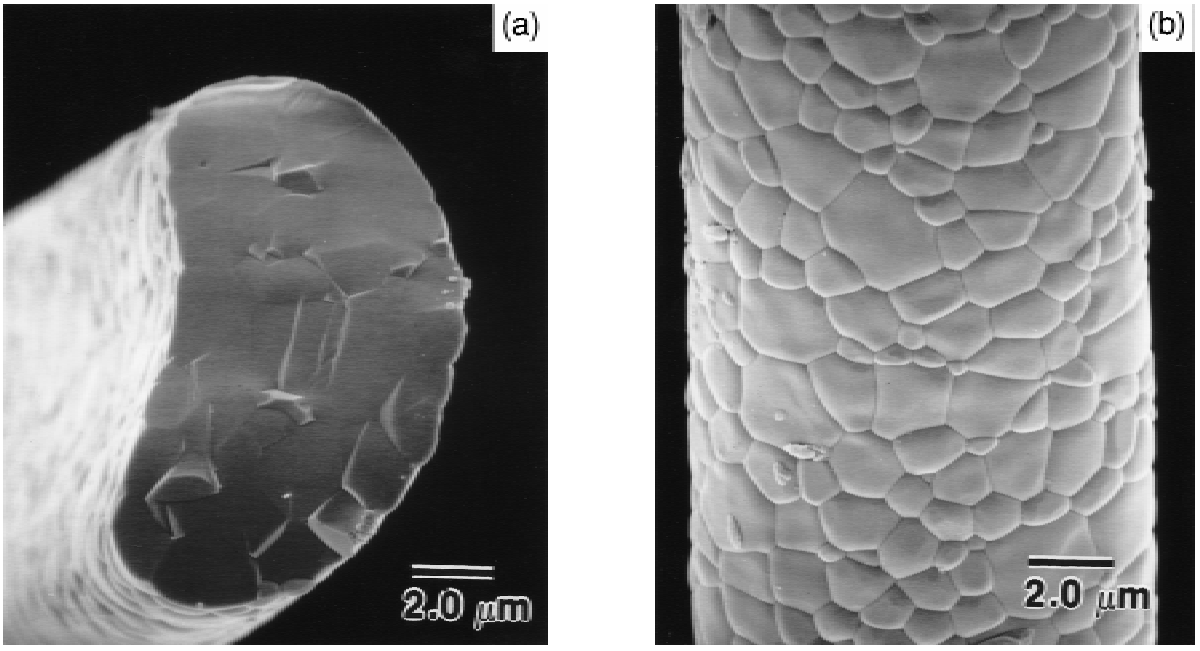

Fig. 27. SEM micrographs of extruded YAG formate/acetate precursor fiber heated at 1°C/min to 100°C for 2 h, 1°C/min to 400°C for 2 h, 15°C/min to 900°C for 2 h, and then 30°C/min to 1600°C for 2 h.

sible explanation is that, at 1570°C, the fibers are not completely dense and have a higher flaw population, which leads to bend strengths that are lower than those of 1600°C fibers. However, SEM studies on fracture surfaces of fibers that have been sintered at 1570°C show porosities of <0.7% (point-fraction analysis).

Although pores were not observed at initial fracture positions, we cannot as yet exclude their role as critical flaws. An alternate explanation is that the large, irregular grain boundaries at the fiber surfaces serve as critical flaws. More work needs to be performed to identify the exact source(s) of failure. Compared to the YAG fibers that were prepared by King *et al.*[10a] (bend strength of 520 ± 180 MPa), thinner YAG fibers with smaller average crystallite sizes seem to offer higher bend strengths (1.7 ± 0.2 GPa). Additional work is required to fully validate these conclusions and to analyze the creep properties.

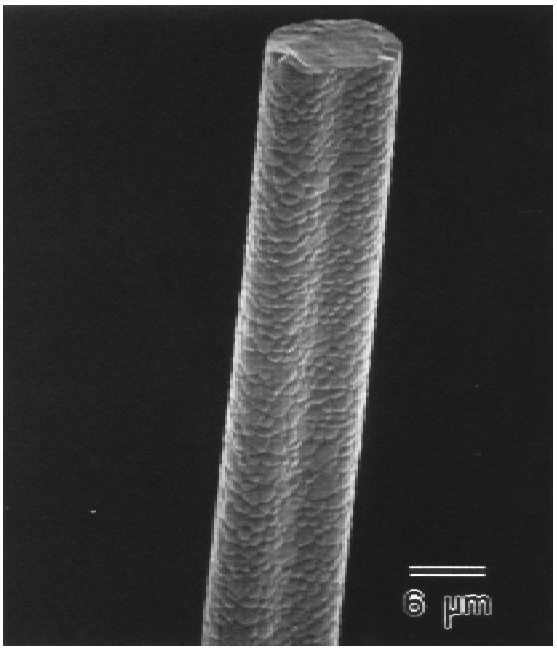

Fig. 28. SEM micrograph of extruded YAG formate/acetate precursor fiber heated at 1°C/min to 100°C for 2 h, 1°C/min to 400°C for 2 h, 15°C/min to 900°C for 2 h, and then 30°C/min to 1570°C for 2 h; a bending test shows that the fiber has a bend strength of 1.3 ± 0.2 GPa.

IV. Conclusions

The chemical evolution that occurs during the pyrolytic transformation of bulk samples of $Al(O_2CH)_3 \cdot 3H_2O$ and $Y(O_2CCH_3)_3 \cdot 4H_2O$ to their respective, common high-temperature ceramic forms, α-Al_2O_3 and bcc Y_2O_3, was examined. The results established baseline behavior patterns of use in evaluating the decomposition patterns of a YAG precursor that was formulated from 5:3 stoichiometric mixtures of $Al(O_2CH)_3 \cdot 3H_2O$, $Y(O_2CCH_3)_3 \cdot 4H_2O$, and additives. In the individual cases, decomposition followed well-defined pathways, wherein the initial products were the amorphous oxides that were contaminated with trace-to-minor amounts of the respective carbonates. At higher temperatures, the ceramic

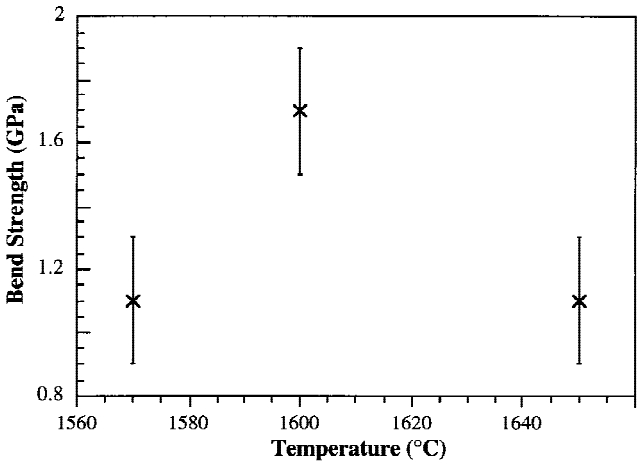

Fig. 29. Bend strength versus sintering temperature.

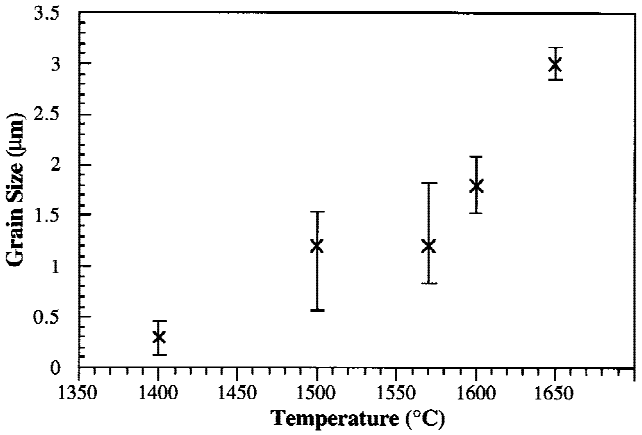

Fig. 30. Grain size versus sintering temperature.

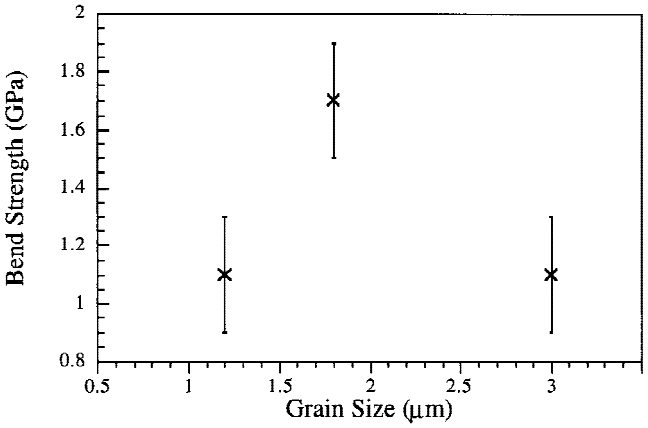

Fig. 31. Bend strength versus grain size.

products crystallized: for $Al(O_2CH)_3 \cdot 3H_2O$, first η-Al_2O_3 (840°C) and then α-Al_2O_3 (>1120°C); for $Y(O_2CCH_3)_3 \cdot 4H_2O$, only bcc Y_2O_3 ($\geq$400°C). Surprisingly, these results had almost no bearing on the reactivity pattern of the YAG precursor, which behaved like a separate compound and decomposed to crystalline YAG at ~800°C without any phase separation.

Finally, isobutyrate and acetate/formate YAG precursors were both easily spun or hand drawn to form well-defined green fibers. The thicker extruded fibers exhibited excessive cracking and foaming when efforts were made to form ceramic fibers, which can be attributed to the subsurface buildup of gases during the conversion process. Thinner green fibers (<30 μm) are easily converted to fully dense ceramic fibers at temperatures $\geq$1570°C. The best bend strength for these fibers is 1.7 ± 0.2 GPa (1600°C sintering), which is a factor of ~3 greater than that found for polycrystalline YAG fibers in previous studies.

References

[1]Y. Liu, Z.-F. Zhang, B. King, J. W. Halloran, and R. M. Laine, ''Synthesis of Yttrium Aluminum Garnet from Yttrium and Aluminum Isobutyrate Precursors,'' *J. Am. Ceram. Soc.*, **79** [2] 385–94 (1996).

[2](a) G. S. Corman, ''High-Temperature Creep of Some Single Crystal Oxides,'' *Ceram. Eng. Sci. Proc.*, **12** [9–10] 1745–66 (1991). (b) T. A. Parthasarathy, T. Mah, and K. Keller, ''High-Temperature Deformation Behavior of Polycrystalline Yttrium Aluminum Garnet (YAG),'' *Ceram. Eng. Sci. Proc.*, **12** [9–10] 1767–73 (1991).

[3]E. M. Levin, C. R. Robbins, and H. F. McMurdie, *Phase Diagrams for Ceramists;* p. 122. American Ceramic Society, Columbus, OH, 1969.

[4]A. H. Chokshi and J. R. Porter, ''Analysis of Concurrent Grain Growth During Creep of Polycrystalline Alumina,'' *J. Am. Ceram. Soc.*, **69** [2] C-37–C-39 (1986).

[5]D. Hull, *An Introduction to Composite Materials;* pp. 1–8. Edited by R. W. Cahn, E. A. Davis, and I. M. Ward. Cambridge University Press, Cambridge, U.K., 1985.

[6](a) F. T. Wallenberger, N. E. Weston, and S. A. Dunn, ''Inviscid Melt Spinning: As-Spun Crystalline Alumina Fibers,'' *J. Mater. Res.*, **5** [11] 2682–86 (1990). (b) F. T. Wallenberger, N. E. Weston, K. Motzfeldt, and D. G. Swartzfager, ''Inviscid Melt Spinning of Alumina Fibers: Chemical Jet Stabilization,'' *J. Am. Ceram. Soc.*, **75** [3] 629–36 (1992). (c) F. T. Wallenberger, ''Melt Spinning of Amorphous Alumina Fibers,'' *Am. Ceram. Soc. Bull.*, **69** [10] 1646–48 (1990).

[7]T. F. Cooke, ''Inorganic Fibers—A Literature Review,'' *J. Am. Ceram. Soc.*, **74** [12] 2959–78 (1991).

[8]L. E. Seulert, ''Alumina Fiber,'' U.S. Pat. No. 3 808 015, 1974.

[9]Z.-F. Zhang, ''Processing Silicon Carbide Fibers from Organosilicon Precursors''; Ph.D. Dissertation. The University of Michigan, Ann Arbor, MI, 1994.

[10](a) B. H. King, Y. Liu, R. M. Laine, and J. W. Halloran, ''Fabrication of Yttrium Aluminate Fibers,'' *Ceram. Eng. Sci. Proc.*, **14** [7–8] 639–50 (1993). (b) S. D. Nunn, D. Popovic, S. Baskaran, J. W. Halloran, G. Subramanian, and S. G. Bike, ''Suspension Dry Spinning and Rheological Behavior of Ceramic-Powder-Loaded Polymer Solutions,'' *J. Am. Ceram. Soc.*, **76** [10] 2460–64 (1993).

[11]G. Gowda, ''Synthesis of Yttrium Aluminates by the Sol–Gel Process,'' *J. Mater. Sci. Lett.*, **5**, 1029–32 (1986).

[12](a) R. M. Laine, K. A. Youngdahl, R. A. Kennish, M. L. Hoppe, Z.-F. Zhang, and D. J. Ray, ''Superconducting Fibers from Organometallic Precursors, Part II: Chemistry and Low Temperature Processing,'' *J. Mater. Res.*, **6**, 895 (1991). (b) Z.-F. Zhang, R. A. Kennish, K. A. Blohowiak, M. L. Hoppe, and R. M. Laine, ''Superconducting Fibers From Organometallic Precursors. Part III. High Temperature Pyrolytic Processing,'' *J. Mater. Res.*, **8**, 1777–90 (1993). (c) R. M. Laine and K. A. Youngdahl, U.S. Pat. No. 5 071 833, 1993.

[13]R. S. Hay, ''Phase Transformations and Microstructure Evolution in Sol–Gel Derived Yttrium-Aluminum Garnet Films,'' *J. Mater. Res.*, **8**, 578–604 (1993).

[14]R. Baranwal, A. Zika, B. L. Mueller, and R. M. Laine, ''Preceramic Polymer Routes to Amorphous and Crystalline Aluminosilicate Powders for Electrorheological Applications. I.''; pp. 157–69 in *Progress in Electrorheology.* Edited by K. Havelka and F. E. Filisko. Plenum Press, New York, 1995.

[15](a)S. Yajima, ''Synthesis of a Polytitanocarbosilane and Its Conversion into Inorganic Compounds,'' *J. Mater. Sci.*, **16**, 1349–55 (1981). (b) S. Yajima, ''Special Heat-Resisting Materials from Organometallic Polymers,'' *Am. Ceram. Soc. Bull.*, **62** [8] 893–98 (1983).

[16]J. C. Romine, ''Aluminum Oxide Fibers''; pp. 151–75 in *Handbook of Fiber Science and Technology: Vol. III, High Technology Fibers Part B.* Edited by M. Lewin and J. Preston. Marcel Dekker, New York, 1983.

[17]Sumitomo Chemical Industries, Jpn. Pat. Nos., 83 98 428 and 58 98 428, 1983.

[18]D. D. Johnson, *J. Coated Fabr.*, **11**, 282 (1981).

[19]G. F. Everitt, ''Stabilized Aluminum Acetate Used for an Alumina Source in Ceramic Fibers''; in *Ultrastructure Processing of Advanced Ceramics.* Edited by J. D. Mackenzie and D. R. Ulrich. Wiley, New York, 1988.

[20]H. G. Sowman and T. T. Tran, ''Refractory Fibers of Alumina and Amorphous Phosphorus Pentoxide,'' U.S. Pat. No. 4 801 562, 1989.

[21]T. E. Wood and D. M. Wilson, ''Microcrystalline Alumina-Based Ceramic Articles,'' U.S. Pat. No. 4 954 462, 1990.

[22](a) H. G. Sowman, ''Refractory Fibers of Alumina and Organic Residue,'' U.S. Pat. No. 4 929 578, 1990. (b) D. M. Wilson, D. C. Lueneburg, and S. L. Lieder, ''High Temperature Properties of Nextel 610 and Alumina-Based Nanocomposite Fibers,'' *Ceram. Eng. Sci. Proc.*, **14** [7–8] 609–21 (1993).

[23](a) K. Pallavi; unpublished paper on mullite fibers. (b) G. D. Soraru, M. Mercadini, R. D. Maschio, F. Taulelle, and F. Babonneau, ''Si-Al-O-N Fibers from Polymeric Precursor: Synthesis, Structural, and Mechanical Characterization,'' *J. Am. Ceram. Soc.*, **76** [10] 2595–600 (1993). (c) O. Funayama, H. Nakahara, A. Tezuka, T. Ishii, and T. Isoda, ''Development of Si-B-O-N Fibers from Polyborosilazane,'' *J. Mater. Sci.*, **29**, 2238–44 (1994). (d) D. B. Marshall, F. F. Lange, and P. D. Morgan, ''High-Strength Zirconia Fibers,'' *J. Am. Ceram. Soc.*, **70** [8] C-187–C-188 (1987). (e) M. E. P. Fernandez, C. Kang, and P. L. Mangonon, ''Processing Ceramic Fibers by Sol–Gel,'' *Chem. Eng. Prog.*, **89** [9] 49–53 (1993). (f) G. Emig, R. Wirth, and R. Zimmermann-Chopin, ''Sol/Gel-Based Precursors for Manufacturing Refractory Oxide Fibers,'' *J. Mater. Sci.*, **29**, 4559–66 (1994).

[24](a) J. Yang, S. M. Jeng, and S. Chang, ''Fracture Behavior of Directionally Solidified $Y_3Al_5O_{12}/Al_2O_3$ Eutectic Fiber,'' *J. Am. Ceram. Soc.*, **79** [5] 1218–22 (1996). (b) T. Mah, T. A. Parthasarathy, and L. E. Matson, ''Processing and Properties of $Al_2O_3/Y_3Al_5O_{12}$ (YAG) Eutectic Composite,'' *Ceram. Eng. Sci. Proc.*, **11** [9–10] 1617 (1990).

[25](a) B. M. Tissue, W. Jia, L. Lu, and W. M. Yen, ''Coloration of Chromium-Doped Yttrium Aluminum Garnet Single-Crystal Fibers Using a Divalent Codopant,'' *J. Appl. Phys.*, **70** [7] 3775–77 (1991). (b) G. S. Corman, ''Strength and Creep of Single Crystal YAG Fibers''; presented at the 94th Annual Meeting of the American Ceramic Society, Minneapolis, MN, April 12–16, 1992 (Paper No. 64-SII-92).

[26]G. N. Morscher, K. C. Chen, and K. S. Mazdiyasni, ''Creep-Resistance of Developmental Polycrystalline Yttrium-Aluminum Garnet Fibers,'' *Ceram. Eng. Sci. Proc.*, **14** [7–8] 181–88 (1994).

[27]Y. Liu, B. H. King, Z.-F. Zhang, J. W. Halloran, and R. M. Laine, ''Creep Resistant Oxide Fibers,'' Paper No. WL-TR-94-4100, Materials Directorate, Wright Laboratory, Air Force Material Command, Wright-Patterson AFB, OH, March 1994.

[28]B. H. King and J. W. Halloran, ''Polycrystalline Yttrium Aluminum Garnet Fibers from Colloidal Sols,'' *J. Am. Ceram. Soc.*, **78** [8] 2141–48 (1995).

[29]P. A. Siemers, R. L. Mehan, and H. Moran, ''A Comparison of the Uniaxial Tensile and Pure Bending Strength of SiC Filaments,'' *J. Mater. Sci.,* **23**, 1329–33 (1988).

[30]J. T. Kwon, ''Aluminum Formate: Part I, The Synthesis of Aluminum Formates. Part II, The Pyrolysis Reactions of Aluminum Formates''; Ph.D Dissertation; pp. 9–19. Cornell University, New York, 1963.

[31]N. M. Chaplygina, I. Z. Babievskaya, and I. B. Kudinov, ''Preparation and Physicochemical Properties of $Al(HCOO)_3 \cdot 3H_2O$,'' *Russ. J. Inorg. Chem.* (*Engl. Transl.*), **29** [9] 1260–63 (1984).

[32]T. Sato, ''Thermal Decomposition of Inorganic and Organic Acid Salts of Aluminum and Thermal Transformation of the Formed Aluminas,'' *Netsu Sokutei*, **13** [3] 113–22 (1986).

[33]L. M. Seaverson, S.-Q. Luo, P.-L. Chien and J. F. McClelland, ''Carbonate Associated with Hydroxide Sol–Gel Processing of Yttria: An Infrared Spectroscopic Study,'' *J. Am. Ceram. Soc.,* **69** [5] 423–29 (1986).

[34]G. A. M. Hussein, ''Formation of High Surface-Area Yttrium Oxide by the Thermal Decomposition of Different Inorganic Precursors,'' *Thermochim. Acta,* **244**, 139–51 (1994).

[35]V. N. Maksimov, K. N. Semenenko, T. N. Naumova, and A. V. Novoselova, ''The Aluminum Acetates,'' *Russ. J. Inorg. Chem.* (*Engl. Transl.*), **5** [3] 267–70 (1960).

[36]W. Weng, J. Yang, and Z. Ding, ''The Sol–Gel Process of the Yttrium Complex from Yttrium Acetate,'' *J. Non-Cryst. Solids,* **169**, 177–82 (1994).

[37]P. Apte, H. Burke, and H. Pickup, ''Synthesis of Yttrium Aluminum Garnet by Reverse Strike Precipitation,'' *J. Mater. Res.,* **7** [3] 706–11 (1992).

[38]V. Lavaste, J. Besson, M. Berger, and A. R. Bunsell, ''Elastic and Creep Properties of Alumina-Based Single Fibers,'' *J. Am. Ceram. Soc.,* **78** [11] 3081–87 (1995).

[39]D. J. Pysher and R. E. Tressler, ''Creep Rupture Studies of Two Alumina-Based Ceramic Fibers,'' *J. Mater. Sci.,* **27**, 423–28 (1992). □